Metabolism of sphingadiene and characterization of the sphingadiene-producing enzyme FADS3

Keisuke Jojima, Akio Kihara*

Faculty of Pharmaceutical Sciences, Hokkaido University, Sapporo 060-0812, Japan

*Correspondence to:

Akio Kihara

Laboratory of Biochemistry, Faculty of Pharmaceutical Sciences

Hokkaido University

Kita 12-jo, Nishi 6-chome, Kita-ku, Sapporo 060-0812, Japan

Tel: +81-11-706-3754

Fax: +81-11-706-4900

E-mail addresses: kihara@pharm.hokudai.ac.jp

Abstract

Of the long-chain bases (LCBs) that comprise the ceramides (CERs) present in mammals, only 4,14-sphingadiene (sphingadiene; SPD) has a *cis* double bond (at C14). Because of this unique structure, the metabolism of SPD may differ from that of other LCBs, but whether this is the case remains unclear. FADS3 is responsible for introducing the *cis* double bond in SPD. However, the substrate specificity of FADS3 and cofactors involved in the FADS3-catalyzed reaction are also unknown. In the present study, a cell-based assay using a ceramide synthase inhibitor and an *in vitro* experiment showed that FADS3 is active toward sphingosine (SPH)-containing CERs (SPH-CERs) but not toward free SPH. FADS3 exhibits specificity with respect to the chain length of the SPH moiety of SPH-CERs (active toward C16–20), but not that of the fatty acid moiety. Furthermore, FADS3 is active toward straight-chain and *iso*-branched-chain SPH-containing CERs but not toward *anteiso*-branched forms. In addition to SPH-CERs, FADS3 also shows activity toward dihydrosphingosine-containing CERs, but this activity is approximately half of that toward SPH-CERs. It uses either NADH or NADPH as an electron donor, and the electron transfer is facilitated by cytochrome b_5. The metabolic flow of SPD to sphingomyelin is predominant over that to glycosphingolipids. In the metabolic pathway from SPD to fatty acids, the chain length of the SPD is reduced by two carbons and the *trans* double bond at C4 is saturated. This study thus elucidates the enzymatic properties of FADS3 and the metabolism of SPD.

Key words

Ceramide, Desaturase, Lipid metabolism, 4,14-Sphingadiene, Sphingolipid.

Abbreviations

CER, ceramide; *d*, deuterium; DHS, dihydrosphingosine; FA, fatty acid; FADS, fatty acid desaturase; FB_1, fumonisin B_1; 6-OH, 6-hydroxy; KO, knockout; LC, liquid chromatography;

LCB, long-chain base; MRM, multiple reacting monitoring; MS/MS, tandem mass spectrometry; PHS, phytosphingosine; SM, sphingomyelin; SPH, sphingosine; SPT, serine palmitoyltransferase.

1. Introduction

Sphingolipids are multifunctional lipids present in eukaryotes and some prokaryotes [1]. As constituents of biological membranes, components of multilayered lipid structures in skin, or lipid mediators, they play roles in a variety of physiological functions, including neural function, skin barrier formation, immunity, spermatogenesis, and regulation of sugar metabolism [1-4]. Sphingolipids are abundant in the plasma membranes and form lipid microdomains, which, together with cholesterol, serve as platforms for proteins involved in signal transduction [5].

The hydrophobic backbone of sphingolipids is ceramide (CER), which is composed of a long-chain amino alcohol called a long-chain base (LCB) and a fatty acid (FA). Complex sphingolipids have a polar head group, which, in mammals, is a phosphocholine (in sphingomyelin [SM]) or carbohydrate(s) (in glycosphingolipids). The combination of these three components (LCB, FA, and polar head group), each of which can take various forms, creates a vast number of molecular species of sphingolipids [1], and this structural diversity is the molecular basis for their multifunctional properties.

The LCBs commonly have hydroxyl groups at C1 and C3 and an amino group at C2. These functional groups act as electron donors and acceptors for hydrogen bonds that are important for the lipid–lipid interactions in lipid microdomain formation [6, 7]. Mammals have five types of LCBs: dihydrosphingosine (DHS), sphingosine (SPH, which has a *trans*-double bond at C4), phytosphingosine (PHS, which has a hydroxyl group at C4), 6-hydroxy (6-OH) SPH (which has a *trans*-double bond at C4 and a hydroxyl group at C6), and 4,14-sphingadiene (SPD; which has *trans*- and *cis*-double bonds at C4 and C14, respectively) [1, 8]. SPH, DHS, and SPD are distributed throughout a wide range of tissues, whereas PHS and 6-OH SPH are tissue-specific (PHS: epithelial tissues such as epidermis, small intestine, and kidney; 6-OH SPH: epidermis) [1, 9-13]. These two types of LCBs, which have one more hydroxyl group than the other three, may enhance permeability barrier function by strengthening lipid–lipid

interactions in epithelial tissues. In contrast, SPD—the only mammalian LCB with a *cis*-double bond—weakens lipid–lipid interactions because of the angled nature of the *cis*-double bond, preventing localization of SPD-containing sphingolipids to the lipid microdomain [12]. In addition, the presence of the *cis*-double bond in SPD may mean that there are differences between the metabolism of SPD and SPD-containing CERs (SPD-CERs) from that of other LCBs/CERs, although this has not yet been examined.

FADS3, a member of the FA desaturase (FADS) family, is responsible for the introduction of the *cis*-double bond at C14 in SPD [12, 14]. In humans, the FADS family has eight members: FADS1, FADS2, FADS3, SCD5 (FADS4), SCD1 (FADS5), FADS6, DEGS1 (FADS7), and DEGS2 (FADS8) [15, 16], and of these, only the function of FADS6 remains unknown. FADS1, FADS2, SCD1, and SCD5 are acyl-CoA desaturases that introduce a *cis*-double bond into acyl-CoAs: FADS1 at C5; FADS2 at C6; SCD1 and SCD5 at C9 [17, 18]. In contrast, the substrates of DEGS1 and DEGS2 are DHS-containing CERs (DHS-CERs). DEGS1 introduces a *trans*-double bond at C4 of the DHS moiety of DHS-CERs to generate SPH-containing CERs (SPH-CERs) [15]. DEGS2 is a bifunctional enzyme with C4-hydroxylase activity and weak C4-desaturase activity, producing PHS-containing CERs and SPH-CERs, respectively [13, 15, 19]. Although we have previously reported that FADS3 produces SPD-CERs, using SPH-CERs as substrates [12], another study has shown that FADS3 also exhibits activity toward free SPH (as well as SPH-CERs) [14]. Thus, the precise substrates of FADS3 remain controversial.

The desaturation/hydroxylation reactions catalyzed by FADS family members are initiated via the transfer of an electron from NADH or NADPH to cytochrome b_5 reductases [17, 19]. The electron is then transferred to cytochrome b_5 and thereafter to FADS proteins, resulting in the desaturation/hydroxylation of the substrate and the conversion of molecular oxygen to water. Of the FADS family members, FADS1–3 have their own cytochrome b_5-like domains [20]. Although FADS2 can catalyze the desaturation reaction in the absence of cytochrome b_5, this activity is enhanced in its presence [21]. It is unclear, however, whether

FADS3-catalyzed reactions are also enhanced by cytochrome b_5.

The first reaction in sphingolipid biosynthesis is the condensation of serine with acyl-CoA to produce 3-ketodihydrosphingosine. Serine palmitoyltransferases (SPTs), which catalyze this reaction, are composed of large subunits (SPTLC1, SPTLC2, and SPTLC3) and small subunits (SPTSSA and SPTSSB) [22]. There are four SPT complexes with different combinations of these subunits: SPTLC1/SPTLC2/SPTSSA, SPTLC1/SPTLC2/SPTSSB, SPTLC1/SPTLC3/SPTSSA, and SPTLC1/SPTLC3/SPTSSB. Each of these exhibits characteristic substrate specificity in terms of acyl-CoA chain lengths [23-26]. Certain mutations in *SPTLC1* or *SPTLC2* cause hereditary sensory neuropathy type 1 (HSAN1) [22]. These mutations alter the substrate specificity of SPT so that it uses alanine or glycine as its substrate, which causes the production of the neurotoxic 1-deoxy sphingolipids [22, 27, 28]. FADS3 is involved in the production of 1-deoxy-14*Z*-SPH, a metabolite of 1-deoxy-sphingolipids [14, 29].

The quantities of sphingolipids required in a tissue are maintained by a balance between synthesis and degradation. CERs are synthesized in the endoplasmic reticulum, converted to complex sphingolipids (SMs and glycosphingolipids) in the Golgi apparatus, and transported to the plasma membrane [1, 30, 31]. In contrast, the degradation of sphingolipids occurs mainly in lysosomes, where sphingolipids are degraded to LCBs [31]. These LCBs are then either recycled for sphingolipid synthesis or converted to FAs (via LCB 1-phosphates and fatty aldehydes) that are incorporated mainly into glycerophospholipids [1, 32]. Metabolic flows differ among LCBs: while SPH and DHS are either metabolized to both SMs and glycosphingolipids or degraded to saturated FAs with two shorter carbon chains [32, 33], the efficiency of PHS-to-SM metabolism is low, so most PHS is metabolized to glycosphingolipids [34, 35]. In the degradation pathway, PHS undergoes α-oxidation and is converted to an FA with three shorter carbon chains [34, 35]. However, the details of the metabolism of SPD are unknown.

As described above, the substrate specificity and cytochrome b_5 dependence of FADS3 are unclear. In addition, the metabolic flow of SPD to complex sphingolipids and the degradation pathway of SPD remain undetermined. In the present study we resolve these questions and provide clues to the molecular mechanism of sphingolipid homeostasis.

2. Material and methods

2.1. Mice

Male C57BL/6J mice purchased from Sankyo Laboratory Services (Tokyo, Japan) were used in this study. They were maintained under a room temperature of 23 ± 1 °C, humidity of 50 ± 5%, and a 12-hour light/dark cycle with free access to a standard chow diet (PicoLab Rodent Diet 20; LabDiet, St. Louis, MO) and water. The animal experiments were approved by the institutional animal care and use committee of Hokkaido University.

2.2. Cells, growth conditions, and transfection

We cultured HEK 293T cells (RIKEN BioResource Research Center, Tsukuba, Japan) and myelogenous leukemia-derived human HAP1 cells (American Type Culture Collection, Manassas, VA) in Dulbecco's modified Eagle's medium (D6429; Merck, Darmstadt, Germany) and Iscove's modified Dulbecco's medium (Thermo Fisher Scientific, Waltham, MA), respectively, both containing 10% fetal bovine serum, 100 units/mL penicillin, and 100 μg/mL streptomycin (Merck) at 37 °C under 5% CO_2. HEK 293T cells were grown on dishes coated with 3% collagen (Cellmatrix Type I-P; Nitta gelatin, Osaka, Japan). *FADS3* KO HAP1 cells were generated as previously reported [12]. *DEGS1* KO HAP1 cells were generated using the CRISPR/Cas9 system as described previously [36], and a clone with a 33 bp deletion in exon 2 of *DEGS1* was obtained and used. Transfections were performed using Lipofectamine Transfection Reagent with PLUS Reagent (Thermo Fisher Scientific), according to the manufacturer's instructions.

2.3. Plasmids

The mammalian expression vectors pCE-puro 3×FLAG-1 and pCE-puro HA-1 were used to express proteins with 3×FLAG tag and HA tag, respectively, at the N-termini [37 50, 38]. The pCE-puro 3×FLAG-FADS3, pCE-puro 3×FLAG-CERS1–6, pCE-puro 3×FLAG-ELOVL1,

pCE-puro 3×FLAG-SPTLC1, pCE-puro 3×FLAG-SPTSSB, and pCE-puro HA-SPTLC3 plasmids have been described previously [12, 26, 39]. The pCE-puro 3×FLAG-CYB5A plasmid was constructed as follows. The human *CYB5A* gene was first amplified from human kidney cDNA (Takara Bio, Shiga, Japan) via PCR using the following primers: 5′-GGATCCATGGCAGAGAGCAGTCGGACGAGGCC-3′ and 5′-TCAGTCCTCTGCCATGTATAGGCT-3′. The amplified gene was cloned into the TA cloning vector pGEM-T Easy (Promega, Madison, WI) and then transferred to the pCE-puro-3×FLAG-1 vector.

2.4. Immunoblotting

Immunoblotting was performed as described previously [35]. Anti-FLAG monoclonal antibody (M2; 1 μg/mL; Merck), anti-HA monoclonal antibody (HA-7; 1 μg/mL; Merck), and anti-GAPDH monoclonal antibody (5A12; 0.5 μg/mL; FUJIFILM Wako Pure Chemical, Osaka, Japan) were used as the primary antibodies. Anti-mouse IgG HRP-conjugated $F(ab')_2$ fragment (1/7,500 dilution; Cytiva, Marlborough, MA) was used as the secondary antibody. A chemiluminescence solution consisting of 100 mM Tris-HCl (pH 8.5), 0.2 mM *p*-coumaric acid (Merck), 2.5 mM luminol (FUJIFILM Wako Pure Chemical), and 0.02% hydrogen peroxide was used to detect chemiluminescence.

2.5. Lipid analyses

Liquid chromatography (LC)-tandem mass spectrometry (MS/MS) analyses were performed using an ultra performance LC-coupled triple quadrupole mass spectrometer (Xevo TQ-S; Waters, Milford, MA). LC separations were performed on a Triart C18 (metal-free column, length 150 mm, particle size 1.9 μm, inner diameter 2.1 mm; YMC, Kyoto, Japan) or ACQUITY UPLC CSH C18 column (length 100 mm, particle size 1.7 μm, inner diameter 2.1 mm; Waters) with a column temperature of 55 °C and a flow rate of 0.3 mL/min in a binary

gradient system using mobile phase A (acetonitrile/water [3:2, v/v]) and mobile phase B (2-propanol/acetonitrile [9:1, v/v], both containing 5 mM formic acid ammonium). Lipids separated by LC were ionized by electrospray ionization and analyzed by MS/MS in multiple reacting monitoring (MRM) mode. The *m/z* values of the precursor and product ions of each lipid species were set at Q1 and Q3 (Table S1), respectively, and detected in positive ion mode. The quantity of each lipid was calculated by comparing the peak area of the mass spectrogram to that of an internal (for the measurements of most of the lipids in this study) or external standard (for seven deuterium [d_7]-containing SPH and d_7-SPD measurements). We used d_9-SPH-CER (*N*-palmitoyl d_9-D-*erythro*-SPH [d18:1/d_9-C16:0]; catalog number 791660; Avanti Polar Lipids, Alabaster, AL) as an internal standard for the quantification of SPD-CERs. The validity of the use of this standard has been reported previously: SPD-CER and SPH-CER show different retention times in LC and similar fragmentation patterns and peak intensities in fragmentation analysis, but each produces a major fragment peak with a characteristic *m/z* value (SPD, 262.3; SPH, 264.3) [12]. For the same reason, SPH-containing SM (d_9-SM [d18:1/d_9-C16:0; catalog number 27551; Cayman Chemical, Ann Arbor, MI] or C12:0 SM [d18:1/C12:0; catalog number LM6005; Avanti Polar Lipids]) and SPH-containing HexCER (d_3-HexCER [d18:1/d_3-C16:0; catalog number 24621; Cayman Chemical] or C12:0 HexCER [d18:1/C12:0; catalog number LM6005; Avanti Polar Lipids]) were used as internal standards for the measurements of SPD-containing SMs and HexCERs. The software MassLynx (Waters) was used for data analysis. Details of each lipid measurement are described below.

Quantification of CERs, SMs, and HexCERs in mouse brain and kidney was performed as follows. Brain and kidney (10 mg) collected from three-month-old mice were transferred to glass tubes containing zirconia beads and mixed with 450 μL chloroform/methanol (1:2, v/v) and internal standards (100 pmol d_9-SPH-CER; 500 pmol [brain] or 100 pmol [kidney] d_3-HexCER; 250 pmol d_9-SM). The tissues were then crushed by vigorous mixing (4,500 rpm, 4 °C, 1 min) using a Micro Smash MS-100 (TOMY Seiko, Tokyo, Japan). After centrifugation

(20,400 × *g*, 4 °C, 3 min), the supernatant was collected. The procedure was repeated for the pellets, and that supernatant was combined with the first one. Samples were then treated with 22.5 µL of 4 M KOH and incubated at 37 °C for 1 h to hydrolyze the ester bonds in the glycerolipids. After neutralization by 22.5 µL of 4 M formic acid, the samples were mixed vigorously with 300 µL chloroform and 540 µL H_2O and centrifuged (20,400 × *g*, room temperature, 3 min) for phase separation. The organic phase containing lipids was collected, dried, dissolved in 500 µL chloroform/methanol (1:2, v/v), diluted to appropriate concentrations, and subjected to LC-MS/MS analyses. LC separation was performed using a Triart C18 column with the following gradient steps (gradient condition 1): 0 min, 40% B; 0–33 min, gradient to 100% B; 33–38 min, 100% B; 38–38.1 min, gradient to 40% B; 38.1–40 min, 40% B. MRM settings (Q1 and Q3 values and collision energies) for SPH-CERs and SPD-CERs were as described previously [26], and those for HexCERs and SMs are shown in Table S1.

Quantification of CERs, SMs, HexCERs, and LCBs from cultured cells was performed as follows. Cells grown in 6- or 12-well dishes were treated with d_7-SPH (catalog number 860657; Avanti Polar Lipids), d_7-DHS (catalog number 860657; Avanti Polar Lipids), d_7-SPD (catalog number 860734; Avanti Polar Lipids), 14*Z*-SPH (catalog number 27019; Cayman Chemical), straight-chain C17:0 FA (catalog number H3500; Merck), *iso*-branched-chain C17:0 FA (catalog number 11-1615; Larodan AB, Solna, Sweden), or *anteiso*-branched-chain C17:0 FA (catalog number M3164; Merck). Cells were collected using a scraper, transferred to glass tubes, centrifuged, and suspended in 150 µL of water. Samples were divided into a 50 µL aliquot for protein quantification and a 100 µL aliquot for lipid analyses. Protein quantification was performed using the Pierce BCA Protein Assay Kit (Thermo Fisher Scientific) according to the manufacturer's instructions. For lipid analyses, samples were mixed with 375 µL chloroform/methanol (1:2, v/v) and internal standards (1 or 2 pmol d_9-SPH-CER [for SPH-CER and SPD-CER measurements]; 1 or 2 pmol d_9-DHS-CER [catalog number 791661; Avanti

Polar Lipids; for 14*Z*-SPH-CER measurement]; and 25 pmol LIPIDMAPS Mass Spec Internal Standard, Ceramide/Sphingoid Internal Standard Mix II [catalog number LM6005; Avanti Polar Lipids; C12:0 SM and C12:0 GlcCer in this mixture were used for d_7-SM and d_7-HexCER measurements, respectively]), followed by alkali treatment with KOH, neutralization, phase separation, collection of the organic phase, and drying as described above. The lipids were dissolved in chloroform/methanol (1:2, v/v), diluted to appropriate concentrations, and subjected to LC-MS/MS analyses. LC separation was performed using an ACQUITY UPLC CSH C18 column with the following gradient steps (gradient condition 2): 0 min, 40% B; 0–18 min, gradient to 100% B; 18–23 min, 100% B; 23–23.1 min, gradient to 40% B; 23.1–25 min, 40% B. MRM settings for unlabeled SPH-CERs and SPD-CERs were as described previously [26], and those for unlabeled 14*Z*-SPH-CER and d_7-labeled CERs, HexCERs, SMs, and LCBs are shown in Table S1.

Quantification of FAs was performed as follows. Palmitoleic acid (*cis*-9-C16:1 FA) and *trans*-2-hexadecenoic acid (*trans*-2-C16:1 FA) were purchased from Cayman Chemical (catalog numbers 10009871 and 11132, respectively). Lipids were extracted from cultured cells and alkali-treated as described above. As an internal standard, 50 pmol of d_9-oleic acid (catalog number 86180; Avanti Polar Lipids) was used. Dried lipids were dissolved in 100 μL chloroform/methanol (1:2, v/v), and 1 μL was derivatized with *N*-(4-aminomethylphenyl) pyridinium using the AMP$^+$ Mass Spec Kit (Cayman Chemical), according to the manufacturer's protocol. Samples were diluted with methanol to appropriate concentrations and subjected to LC-MS/MS analyses. Separation by LC was performed using an ACQUITY UPLC CSH C18 column with the following gradient steps (gradient condition 3): 0 min, 10% B; 0–18 min, gradient to 100% B; 18–23 min, 100% B; 23–23.1 min, gradient to 10% B; 23.1–25 min, 10% B. MRM settings are shown in Table S1.

2.6. Measurement of FADS3 activity *in vitro*

Cells suspended in lysis buffer (50 mM HEPES-NaOH [pH 7.4], 150 mM NaCl, 1 mM $MgCl_2$, 1 mM phenylmethylsulfonyl fluoride, and 1 × protease inhibitor cocktail [Complete, EDTA-free protease inhibitor Cocktail; Merck]) were lysed by sonication. After centrifugation (400 × *g*, 4 °C, 3 min), the supernatant (total cell lysates) was collected. Total cell lysates (50 μg) and 10 μM C6-SPH-CER (d18:1/C6:0; catalog number 860506; Avanti Polar Lipids), C6-DHS-CER (d18:0/C6:0; catalog number 860633; Avanti Polar Lipids), or d_7-SPH were mixed in 100 μL of assay buffer (50 mM potassium phosphate [pH 7.5], 1 mM NADH, 1 mM phenylmethylsulfonyl fluoride, and 1 × protease inhibitor cocktail) and incubated at 37 °C for 10 min. After the reaction, 375 μL of chloroform/methanol (1:2, v/v) and internal standard (20 pmol d_9-SPH-CER [for C6-SPD-CER measurement] and 20 pmol d_9-DHS-CER [for C6-14*Z*-SPH-CER measurement]) were added to the samples, which were mixed vigorously, followed by alkali treatment with KOH, neutralization, phase separation, collection of the organic phase, and drying as described above. The lipids thus obtained were dissolved in 200 μL chloroform/methanol (1:2, v/v), diluted to appropriate concentrations, and subjected to LC-MS/MS analyses as described above, using an ACQUITY UPLC CSH C18 column with gradient condition 3. MRM settings for C6-SPD-CER, C6-14*Z*-SPH-CER, and d_7-SPD measurements are shown in Table S1.

3. Results

3.1. Free SPH is not a substrate of FADS3

There are conflicting reports on the substrates of FADS3, with one study suggesting that these are only SPH-CERs [12] and another suggesting that they are both SPH-CERs and free SPH [14]. To clarify this, we first measured the quantity of free SPD in HEK 293T cells overproducing FADS3 with or without the CER synthase inhibitor fumonisin B_1 (FB_1), which causes accumulation of LCBs (the substrates of CER synthases). If FADS3 were active toward free SPH, we would expect that FB_1 treatment would increase the quantity of free SPD. After labeling the cells with d_7-SPH for 4 h, we extracted the lipids and subjected them to measurement of the quantities of free d_7-LCBs (d_7-SPH and d_7-SPD) and d_7-CERs (d_7-SPH-CERs and d_7-SPD-CERs) via LC-MS/MS. In the absence of FB_1, d_7-SPD-CERs were produced in an FADS3 expression-dependent manner (Fig. 1A). Treatment of the cells with FB_1 inhibited the production of CERs (d_7-SPH-CERs and d_7-SPD-CERs) almost completely both in control (vector-transfected cells) and in FADS3-overproducing cells. The levels of free d_7-SPH were comparable between control and FADS3-overexpressing cells in the absence of FB_1 and were similarly increased upon treatment with FB_1. On the other hand, d_7-SPD was below the detection limit in both control and FADS3-overexpressing cells, with or without FB_1 treatment.

Next, we measured the activity of FADS3 toward SPH-CER and free SPH *in vitro*. Total cell lysates prepared from cells transfected with vector or the *FADS3*-encoding plasmid were incubated with SPH-CER containing C6:0 FA (C6-SPH-CER) or d_7-SPH, and the quantities of C6-SPD-CER and d_7-SPD produced were measured via LC-MS/MS. C6-SPD-CER was produced by the lysates prepared from FADS3-overproducing cells at levels that were ~3,000-fold those produced by control lysates (Fig. 1B). However, d_7-SPD was not produced by either of the lysates. Thus, the substrates of FADS3 are SPH-CERs only, and not free SPH, at least under our assay conditions.

3.2. FADS3 exhibits low specificity for the FA chain length of SPH-CERs

Although SPH-CERs include several molecular species that differ in the chain lengths of their FA and/or LCB moieties, the substrate specificity of FADS3 toward these various species is unknown. We therefore first examined its specificity toward FA chain lengths. For this purpose, a 3×FLAG-tagged CER synthase isozyme (CERS1, 2, 3, 4, 5, or 6) was co-overexpressed with 3×FLAG-tagged FADS3 in HEK 293T cells. CERS isozymes show specificity for the chain length of their substrate acyl-CoAs: CERS1, C18:0-CoA; CERS2, C22:0- and C24:0-CoAs; CERS3, ≥C18:0-CoAs; CERS4, C18:0- and C20:0-CoAs; CERS5, C16:0-CoA; CERS6, C16:0-CoA [1, 40-42]. Therefore, overexpressing them results in increases in the CER species with the corresponding FA chain length [43]. The expression levels of CERS1–6 and FADS3 were confirmed by immunoblotting (Fig. 2A). The cells were labeled with d_7-SPH, and the quantities of d_7-SPH-CERs and d_7-SPD-CERs produced were ascertained via LC-MS/MS. In line with a previous report [43], cells overexpressing each CER synthase but not FADS3 exhibited increased levels of the d_7-SPH-CER containing the FA preferred by the respective CER synthase (Fig. 2B). The FA composition of d_7-SPD-CERs in FADS3-overexpressing cells was similar to that of the d_7-SPH-CERs in cells overexpressing the same CER synthase but not overexpressing FADS3.

Since HEK 293T cells contain few SPH-CERs with ≥C26 FAs, we were unable to evaluate the activity of FADS3 toward them in the above experiment. To circumvent this problem, we overexpressed ELOVL1, an FA elongase that produces C26 and C28 acyl-CoAs [39, 44, 45], together with FADS3 and/or CERS3. Immunoblotting confirmed the expression of all these proteins (Fig. 2C). The C26 and C28 acyl-CoAs generated by ELOVL1 led to the production of C26/C28 d_7-SPH-CERs by the CER synthase CERS3, and these were efficiently converted to C26/C28 d_7-SPD-CERs by FADS3 (Fig. 2D). Taken together, these results indicate that FADS3 does not exhibit substrate specificity toward the FA chain lengths of SPH-CERs.

3.3. FADS3 exhibits specificity toward SPH-CERs with C16–20 SPHs

We next examined the substrate specificity of FADS3 toward the SPH chain lengths of SPH-CERs. LCBs can be represented using the number of hydroxyl groups (d, di; t, tri), carbon chain length, and number of double bonds (e.g., d18:1 and d18:2 for SPH and SPD with a carbon chain length of 18, respectively). Hereafter, we use the d/t notation to distinguish them from FAs, for which we use the C notation (e.g., palmitic acid, C16:0). Most of the LCBs in the CERs in most tissues and cells are d18, whereas the brain and epidermis contain CERs with d20 and d/t16–26 LCBs, respectively [26, 46]. The chain length of an LCB is defined by that of its sphingolipid precursor acyl-CoA. SPTs catalyze the condensation of an acyl-CoA (chain-length *n*) with serine to produce 3-ketodihydrosphingosine (*n* + 2), which is then converted to the LCB DHS (*n* + 2). Mammals have four SPT complexes, among which that consisting of the large subunits SPTLC1 and SPTLC3 and a small subunit SPTSSB can use acyl-CoAs with a wide range of chain lengths as substrates [23, 26]. In this study, SPTLC1, SPTLC3, and SPTSSB were co-overexpressed with FADS3 in HEK 293T cells. Their expression was confirmed by immunoblotting (Fig. 3A). SPH-CERs and SPD-CERs with d16–24 were quantified via LC-MS/MS, and all chain lengths other than d23 were detected (Fig. 3B). The levels of SPD-CERs with d16:2–d20:2 were higher in FADS3-overexpressing cells than in vector-transfected cells. In contrast, SPH-CERs with d17:1–d20:1 were reduced by FADS3 overexpression. The levels of SPH-CERs and SPD-CERs with d21, d22, and d24 were low, and FADS3 overexpression did not cause statistically significant changes in these quantities. These results indicate that FADS3 is active toward SPH-CERs with d16:1–d20:1, but not toward those with ≥d21:1.

Although most LCBs in mammals have straight chains, branched-chain LCBs with ω-2 (*iso*) or ω-3 (*anteiso*) methylation are known to exist in some tissues [47, 48]. It has been reported that not only straight-chain but also *anteiso*-branched-chain SPH with d19:1 was produced in HEK 293 cells overexpressing SPTLC3 [47]. In our experiment, we also detected

two adjacent peaks (14.6 min and 14.8 min) on the LC chromatogram for d19:1 SPH-CERs (Fig. 3C). Under our LC conditions using a reversed-phase column, branched-chain SPH-CERs are eluted before straight-chain SPH-CERs, although the peaks of *iso*- and *anteiso*-branched CERs are not separated [48]. Therefore, the 14.6 min and 14.8 min peaks likely correspond to the branched- and straight-chain species, respectively. However, only a single peak was observed for d19:2 SPD-CERs, suggesting that FADS3 is not active toward *anteiso*- and/or *iso*-branched SPH-CERs. To investigate this possibility, we added straight, *iso*-, and *anteiso*-C17:0 FAs (precursors of d19 CERs) to the culture medium of the HEK 293T cells overexpressing SPTLC1, SPTLC3, SPTSSB, and FADS3, and assessed the resulting quantities of d19:1 SPH-CERs and d19:2 SPD-CERs via LC-MS/MS. All types (straight- and *iso/anteiso*-branched-chain) of d19:1 SPH-CERs were detected with or without FADS3 overexpression when their corresponding C17:0 FAs were added (Fig. 3D). Overexpression of FADS3 led to the production of straight-chain and *iso*-branched-chain SPD-CERs with d19:2 but not *anteiso*-branched-chain SPD-CERs. These results indicate that FADS3 is active toward straight-chain and *iso*-branched-chain SPH-CERs, but not toward *anteiso*-branched-chain SPH-CERs. Therefore, the peak of d19:1 SPH-CER, with a retention time of 14.6 min (Fig. 3C), may represent only the *anteiso* form of the branched-chain CER.

3.4. FADS3 is active toward DHS-CERs

DEGS1 encodes the DHS-CER C4 desaturase and is involved in the production of SPH-CERs [15]. In patients with mutations in *DEGS1* and in *DEGS1* knockout (KO) cells, 14*Z*-SPH-containing sphingolipids, which have a *cis*-double bond at C14 but not a *trans*-double bound at C4, are detected [49]. To examine whether 14*Z*-SPH-CERs are produced by FADS3 using DHS-CERs as substrates, we transfected *DEGS1* KO HAP1 cells with vector or the *FADS3*-encoding plasmid, labeled with d_7-DHS, and subjected them to quantification of d_7-14*Z*-SPH-CERs via LC-MS/MS. The levels of d_7-14*Z*-SPH-CERs produced by cells overexpressing

FADS3 were about four-fold those produced by vector-transfected cells (Fig. 4A), indicating that FADS3 is active toward both DHS-CERs and SPH-CERs.

To determine toward which of these FADS3 is more active, we then performed *in vitro* assay combining either C6-DHS-CER (DHS-CER with a C6:0 FA) or C6-SPH-CER as substrates with total cell lysates prepared from HAP1 cells transfected with vector or the *FADS3*-encoding plasmid as enzyme sources. FADS3 produced both C6-14*Z*-SPH-CER and C6-SPD-CER, but the quantity of C6-SPD-CER produced was about double that of C6-14*Z*-SPH-CER (Fig. 4B). Thus, FADS3 exhibits more activity toward SPH-CERs than DHS-CERs.

There are two possible pathways for SPD-CER production. In the first (pathway 1), DHS-CERs are converted to SPH-CERs by DEGS1 and then to SPD-CERs by FADS3 (Fig. 4C). The existence of this pathway is clear, since the activity of DEGS1 and FADS3 toward each of these substrates has already been demonstrated (Fig. 4B) [12, 19]. In the second (pathway 2), DHS-CERs are converted to 14*Z*-SPH-CERs by FADS3 and then to SPD-CERs by DEGS1. Although we had shown that FADS3 can convert DHS-CERs to 14*Z*-SPH-CERs (Fig. 4B), the activity of DEGS1 toward 14*Z*-SPH-CERs had not yet been examined. To investigate this, we incubated HAP1 WT and *DEGS1* KO cells with 14*Z*-SPH to produce 14*Z*-SPH-CERs and then quantified the 14*Z*-SPH-CERs and SPD-CERs produced via LC-MS/MS. In WT cells, SPD-CER production was increased by treatment with 14*Z*-SPH, but this was not the case in *DEGS1* KO cells (Fig. 4D). Instead, quantities of 14*Z*-SPH-CERs in *DEGS1* KO cells were greater than in WT cells. These results suggest that SPD-CERs can also be generated via 14*Z*-SPH-CERs (pathway 2).

3.5. Cytochrome b_5 stimulates the FADS3-catalyzed reaction

To date, it has been unclear whether NADH or NADPH acts as an electron donor in the desaturation reaction catalyzed by FADS3. To investigate this, we examined the activity of FADS3 in the presence of NADH or NADPH, using total cell lysates prepared from HEK 293T

cells overexpressing FADS3 as the enzyme source and C6-SPH-CER as the substrate. The quantity of C6-SPD-CER produced was 14.6- and 12.8-fold higher in the presence of NADH and NADPH, respectively, than in their absence (Fig. 5A), indicating that both NADH and NADPH act as electron donors in the FADS3-catalyzed reaction.

FADS3 has its own cytochrome b_5-like domain. To examine the role of cytochrome b_5 in the FADS3-catalyzed reaction, we co-overproduced the cytochrome b_5 CYB5A, which is localized to the endoplasmic reticulum membrane [50], with FADS3 in HEK 293T cells. The expression of both CYB5A and FADS3 was confirmed by immunoblotting (Fig. 5B). The cells were labeled with d_7-SPH and the quantity of d_7-SPD-CERs generated was examined via LC-MS/MS. Although d_7-SPD-CERs were produced in cells overexpressing FADS3 alone, the quantity was increased 2.1-fold by co-overexpression with CYB5A (Fig. 5C). Thus, cytochrome b_5 promotes the FADS3-catalyzed reaction.

3.6. SPD-CERs are predominantly metabolized to SMs rather than glycosphingolipids

The metabolic flows to complex sphingolipids (SMs and glycosphingolipids) differ among CERs, although that of SPD-CERs was as yet unknown. To reveal this, we labeled *FADS3* KO HAP1 cells with d_7-SPD or d_7-SPH (for comparison) and determined the time course of the production of d_7-labeled CERs, monohexosylceramides (HexCERs; the simplest glycosphingolipids), and SMs via LC-MS/MS. We used *FADS3* KO cells to avoid conversion of SPH to SPD-CERs. The quantities produced and production kinetics of d_7-labeled CERs were similar in d_7-SPH-CERs and d_7-SPD-CERs: both reached a maximum at 5 h after the addition of d_7-SPD/d_7-SPH to the cultures and then decreased (Fig. 6A). HexCER production reached a maximum at 10 h and then decreased under both d_7-SPH and d_7-SPD metabolism. At all times examined except 1 h, the quantities of d_7-SPH-HexCERs produced were greater than those of d_7-SPD-HexCERs (1.7–4.1-fold). In contrast, levels of d_7-SPD-SMs were higher than those of d_7-SPH-SMs (e.g., 1.4-fold at 10 h). The levels of d_7-SPD-SMs increased up to

10 h and then reached a plateau, whereas those of d_7-SPH-SMs increased throughout the measurement period. These results suggest that the metabolism flow of SPD-CERs to SMs is predominant over that to glycosphingolipids.

Next, we examined the quantities of SPD-containing complex sphingolipids in mouse brain and kidney, where SPD-CERs are abundant [12]. The quantities of SPD-CERs were 19.3% and 46.6% of those of SPH-CERs in brain and kidney, respectively (Fig. 6B). Although high levels of SPH-HexCERs (mostly galactosyl CERs) were present in brain, the quantities of SPD-HexCERs were low, accounting for only 3.2% of SPH-HexCERs. In kidney, only trace quantities of HexCERs existed (for both SPH- and SPD-HexCERs), probably because HexCERs are transient metabolic intermediates of more complex glycosphingolipids in this tissue. The quantities of SPD-SMs were 7.2% and 30.0% of those of SPH-SMs in brain and kidney, respectively. The higher levels of SPD-containing SMs than HexCERs relative to their SPH-containing types (7.2% of the SPH-containing SMs vs 3.2% of the SPH-containing HexCERs) in brain are consistent with the above conclusion drawn from the d_7-SPD labeling experiment that metabolism of SPD-CERs to SMs is predominant over that to HexCERs (Fig. 6A).

3.7. SPD is metabolized to mono-unsaturated FAs in the degradation pathway

In the degradation pathway, LCBs are metabolized to acyl-CoAs via several reactions and then incorporated mainly into glycerophospholipids (Fig. 7A) [1]. The metabolism of LCBs to acyl-CoAs is conducted via four common reactions (C1 phosphorylation, C2–C3 cleavage, oxidation [conversion of fatty aldehydes to FAs], and CoA addition) and additional reactions specific to each LCB (SPH, reduction [saturation]; PHS, α-oxidation) [34, 35, 51]. These reactions convert DHS and SPH to 2-carbon shortened, saturated acyl-CoA and PHS to 3-carbon shortened, saturated (non-hydroxylated) acyl-CoA. These acyl-CoAs are used primarily for glycerophospholipid synthesis, either directly or after desaturation/FA elongation.

To reveal the degradation pathway of SPD, we labeled *FADS3* KO cells with d18:2 d_7-SPD or d18:1 d_7-SPH (for comparison) for 0, 1, 5, 10, or 24 h. Lipids were extracted, alkali-treated to release FAs from glycerophospholipids, and subjected to quantification of the d_7-FAs produced via LC-MS/MS. The total quantities of d_7-labeled FAs produced and the kinetics of production were similar with d_7-SPD and d_7-SPH labeling (Fig. 7B). At 1 h of labeling, the most abundant FA species produced from d18:1 d_7-SPH was d_7-C16:0 FA (55.0%), followed by d_7-C18:0 FA (25.1%) and d_7-C18:1 FA (16.2%). Thereafter, the proportion of d_7-C16:0 FA decreased, but that of d_7-C18:1 FA increased. This indicates that d18:1 SPH is first metabolized to C16:0 acyl-CoA and then undergoes FA elongation and desaturation. In contrast, d_7-C16:1 FA was the most abundant FA species produced from d18:2 d_7-SPD at 1 h (52.8%), followed by d_7-C18:1 FA (39.0%) and d_7-C18:2 FA (4.4%). The percentage of d_7-C16:1 FA decreased, but those of d_7-C18:1 FA and d_7-C18:2 FA increased with increasing labeling time. Thus, the first metabolite of d18:2 SPD is C16:1 acyl-CoA, which means that SPD loses only one of its two double bonds (*cis*-14 or *trans*-4) in the degradation pathway to become *cis*-12-C16:1 or *trans*-2-C16:1 acyl-CoA. The LC retention time of d_7-C16:1 FA produced from d18:2 d_7-SPD (4.3 min) was clearly distinct from that of *trans*-2-C16:1 FA (5.6 min) but close to that of *cis*-9-C16:1 FA (4.4 min) (Fig. 7C), indicating that the metabolite of d18:2 SPD is *cis*-12-C16:1 FA. The *trans*-double bond at C4 in SPH is reduced by *trans*-2-enoyl-CoA reductase during metabolism [51]. Our result shows that the *trans*-double bond at C4 in SPD is also reduced in the degradation pathway, with the *cis*-double bond at C14 remaining intact (Fig. 7D).

4. Discussion

In our previous study [12], we proposed that the substrates of FADS3 are SPH-CERs, but not free SPH, based on the following two results. First, the time courses of d_7-SPD-CER synthesis from d_7-SPH and d_7-DHS were similar. Second, C6-SPH-CER was metabolized to C6-SPD-CER in FADS3-overexpressing cells. However, another report also exists that FADS3 is active toward both free SPH and SPH-CERs [14]. The conclusion in that study was drawn from the results of a cell-based assay in the presence of FB_1 and an *in vitro* assay. In the former assay, which used HEK 293 cells labeled with d_7-SPH, the addition of FB_1 reduced the ratio of d_7-SPD to d_7-SPH to ~30%. The finding that the production of d_7-SPD was not completely abolished by the addition of FB_1 led the authors to propose that SPH could also be used as a substrate of FADS3. However, in that experiment, HEK 293 cells that did not overexpress FADS3 were used. Under such conditions (that is, conditions of low FADS3 activity), the d_7-SPD/d_7-SPH ratio was extremely low (~0.03 and ~0.01 before and after the addition of FB_1, respectively), so the activity may not have been accurately evaluated. Indeed, in the present study we could not detect free d_7-SPD with or without FB_1 treatment (Fig. 1A). In the previous *in vitro* assay [14], using total cell lysates prepared from HEK 293 cells overproducing FADS3 as the enzyme source and C6-SPH-CER and d_7-SPH as the substrates, quantities of both C6-SPD-CER and d_7-SPD increased in a 5 min reaction. In that experiment, however, the oxidized form of NAD (NAD^+), not the reduced form (NADH), was used as a coenzyme, which was unable to provide electrons to FADS3. Furthermore, the quantities of C6-SPH-CER and d_7-SPD produced were extremely low (< 0.1% and < 1% of the substrates, respectively), and vector control was also lacking [14]. Our *in vitro* assay showed that 3.5% of the substrate C6-SPH-CER was converted to C6-SPD-CER (Fig. 1B), which indicates that this activity is approximately 50 times stronger than suggested by the previous study [14]. In addition, the activity of FADS3-overproducing cell lysates was ~3,000-fold higher than that of the vector control (Fig. 1B). However, we did not detect any activity of FADS3 toward d_7-SPH *in vitro*.

Our results suggest that the substrates of FADS3 are SPH-CERs but not free SPH, although the possibility that FADS3 exhibits weak activity toward free SPH cannot be completely ruled out. In general, the structure of the polar group of the substrate is important for substrate recognition by the enzyme. The nitrogen-containing moiety of SPH and SPH-CER is an amine and an amide, respectively, and these are completely different in structure: the former is steric while the latter is planar. In addition, the fact that the substrates of DEGS1 (FADS7) and DEGS2 (FADS8), which belong to the same FADS family as FADS3, are DHS-CERs but not free DHS [19], supports our conclusion that the substrates of FADS3 are SPH-CERs but not free SPH. The substrates of the FADS family are not carboxylic acids, ketones, or aldehydes, but carbonyl group-containing thioesters (FADS1, FADS2, SCD5, and SCD1) or amides (FADS3, DEGS1, and DEGS2), suggesting the importance of the carbonyl groups for substrate recognition. Indeed, X-ray crystallography of human SCD1 has shown that the hydrogen atom of the Trp-262 residue and the oxygen atom of the carbonyl group of acyl-CoA are hydrogen bonded [52].

In the present study, we examined the substrate specificity of FADS3 for the chain lengths of the FA and SPH moieties that comprise the SPH-CERs (Figs. 2, 3). FADS3 showed no specificity with respect to the FA moiety and was active toward SPH-CERs with a wide range of chain lengths (C16–C28; Fig. 2). In contrast, it did exhibit specificity with respect to the SPH moiety, and was active only toward d16:1–d20:1 (Fig. 3B). Rat SCD cannot act on acyl-CoAs with ≥C20 [53]. X-ray crystallography of mouse SCD1 shows that it has a hydrophobic tunnel that accommodates the acyl chain, but the limited size of this tunnel may explain its lack of activity toward ≥C20 acyl-CoAs [54]. We speculate that FADS3 has a similar hydrophobic tunnel for the SPH moiety of SPH-CERs, but no such tunnel for the FA moiety (i.e., it may bind to the enzyme's surface), enabling binding to FAs with a wide range of chain lengths. FADS3 showed specificity with respect to not only SPH chain length but also chain branching. It was active toward SPH-CERs with d19:1 straight-chains and *iso*-branched chains, but not toward *anteiso*-branched chains (Fig. 3D). Since the methyl group of *anteiso*-d19:1 SPH at

C16 is adjacent to the site of the enzyme action (introduction of a *cis*-double bond) of FADS3 (between C14 and C15), the steric hindrance of the methyl group may prevent the catalytic groups of FADS3 from carrying out the reaction.

We have shown here that FADS3 is active toward not only SPH-CERs but also DHS-CERs (Fig. 4A and B). Furthermore, DEGS1 exhibited activity toward 14*Z*-SPH-CERs, in addition to the previously known substrates (DHS-CERs; Fig. 4D). These results indicate that SPD-CERs can be produced by both pathway 1, via SPH-CERs, and pathway 2, via 14*Z*-SPH-CERs (Fig. 4C). However, considering that FADS3 activity toward C6-DHS-CER was approximately half of that toward C6-SPH-CER *in vitro* (Fig. 4B), and that 14*Z*-SPH-CERs were barely detectable in WT cells (Fig. 4D), it is highly likely that the predominant SPD synthesis pathway is pathway 1.

The electron donors in the reaction catalyzed by FADS3 were NADH and NADPH (Fig. 5A), similar to other FADS enzymes analyzed thus far [19, 55, 56]. Both cytochrome b_5 reductase and cytochrome P450 oxidoreductase can reduce cytochrome b_5, using mainly NADH and NADPH electrons, respectively [57, 58]. The lack of selectivity for NADH and NADPH in the activity of FADS3 suggests that electrons are supplied from both cytochrome b_5 reductase and cytochrome P450 oxidoreductase to FADS3. FADS3 has its own cytochrome b_5-like domain, as do FADS1 and FADS2. It has been reported that FADS2 is active in the absence of cytochrome b_5, although its activity is enhanced in the presence of cytochrome b_5 [21]. We found that the cytochrome b_5 CYB5A similarly stimulated FADS3 activity (Fig. 5C). This suggests that there are two electron transfer pathways for FADS3: one is the transfer from cytochrome b_5 reductase/cytochrome P450 oxidoreductase directly to the cytochrome b_5-like domain of FADS3, and the other is via cytochrome b_5, with the latter pathway being more efficient than the former.

In this study, we have revealed the metabolic pathways of SPD to complex sphingolipids and acyl-CoAs/FAs. In the former, the metabolism of SPD/SPD-CERs to SMs was

predominant over that to glycosphingolipids (Fig. 6). In the latter, SPD was metabolized to 2-carbon-shortened, mono-unsaturated acyl-CoAs/FAs (Fig. 7). SPD has a *trans*-double bond at the C4, similarly to SPH, and a unique *cis*-double bond at C14. Our study revealed that the double bond present in the acyl-CoAs/FAs corresponds to the *cis*-double bond at C14 in SPD (Fig. 7C). This double bond is located at the C12 position (ω-4) in the C16:1 FA derived from d18:2 SPD, although the presence of such an ω-4 FA has not yet been reported in mammalian cells, probably because of the much lower abundance of the precursor SPD than of glycerophospholipids.

In summary, this study has elucidated the enzymatic properties of FADS3 (cofactor, substrate specificity, and cytochrome b_5 dependence) and the details of SPD metabolism. These findings contribute to the elucidation of the molecular basis of sphingolipid homeostasis. Further studies are needed to elucidate the functions of SPD and its metabolites by analyzing *Fads3* KO mice.

CRediT authorship contribution statement

A. K. conceptualization; K. J. investigation; K. J. and A. K. writing–original draft; A. K. writing–review and editing; A. K., supervision; A. K. project administration; K. J. and A. K. funding acquisition.

Declaration of competing interest

The authors declare that they have no known competing financial interests or personal relationships that could have appeared to influence the work reported in this paper.

Data availability

All data described in this manuscript are contained within the manuscript.

Acknowledgements

We thank Dr. Yusuke Ohno (Hokkaido University) for the useful discussion. This work was supported by Japan Society for the Promotion of Science (JSPS) KAKENHI grant numbers JP22J12598 (to K.J.) and JP22H04986 (to A.K.).

References

[1] A. Kihara, Synthesis and degradation pathways, functions, and pathology of ceramides and epidermal acylceramides, Prog. Lipid Res. 63 (2016) 50–69. https://doi.org/10.1016/j.plipres.2016.04.001.

[2] J. Rivera, R.L. Proia, A. Olivera, The alliance of sphingosine-1-phosphate and its receptors in immunity, Nat. Rev. Immunol. 8 (2008) 753–763. https://doi.org/10.1038/nri2400.

[3] T. Wennekes, R.J. van den Berg, R.G. Boot, G.A. van der Marel, H.S. Overkleeft, J.M. Aerts, Glycosphingolipids—nature, function, and pharmacological modulation, Angew. Chem. Int. Ed. Engl. 48 (2009) 8848–8869. https://doi.org/10.1002/anie.200902620.

[4] M. Rabionet, A. Bayerle, R. Jennemann, H. Heid, J. Fuchser, C. Marsching, S. Porubsky, C. Bolenz, F. Guillou, H.J. Grone, K. Gorgas, R. Sandhoff, Male meiotic cytokinesis requires ceramide synthase 3-dependent sphingolipids with unique membrane anchors, Hum. Mol. Genet. 24 (2015) 4792–4808. https://doi.org/10.1093/hmg/ddv204.

[5] D. Lingwood, K. Simons, Lipid rafts as a membrane-organizing principle, Science 327 (2010) 46–50. https://doi.org/10.1126/science.1174621.

[6] J.P. Slotte, The importance of hydrogen bonding in sphingomyelin's membrane interactions with co-lipids, Biochim. Biophys. Acta 1858 (2016) 304–310. https://doi.org/10.1016/j.bbamem.2015.12.008.

[7] E. Sezgin, I. Levental, S. Mayor, C. Eggeling, The mystery of membrane organization: composition, regulation and roles of lipid rafts, Nat. Rev. Mol. Cell Biol. 18 (2017) 361–374. https://doi.org/10.1038/nrm.2017.16.

[8] S.T. Pruett, A. Bushnev, K. Hagedorn, M. Adiga, C.A. Haynes, M.C. Sullards, D.C. Liotta, A.H. Merrill, Jr., Biodiversity of sphingoid bases ("sphingosines") and related amino alcohols, J. Lipid Res. 49 (2008) 1621–1639. https://doi.org/10.1194/jlr.R800012-JLR200.

[9] M. Iwamori, C. Costello, H.W. Moser, Analysis and quantitation of free ceramide containing nonhydroxy and 2-hydroxy fatty acids, and phytosphingosine by high-

performance liquid chromatography, J. Lipid Res. 20 (1979) 86–96.

[10] K. Nishimura, Phytosphingosine is a characteristic component of the glycolipids in the vertebrate intestine, Comp. Biochem. Physiol. B 86 (1987) 149–154. https://doi.org/10.1016/0305-0491(87)90190-8.

[11] R. t'Kindt, L. Jorge, E. Dumont, P. Couturon, F. David, P. Sandra, K. Sandra, Profiling and characterizing skin ceramides using reversed-phase liquid chromatography-quadrupole time-of-flight mass spectrometry, Anal. Chem. 84 (2012) 403–411. https://doi.org/10.1021/ac202646v.

[12] K. Jojima, M. Edagawa, M. Sawai, Y. Ohno, A. Kihara, Biosynthesis of the anti-lipid-microdomain sphingoid base 4,14-sphingadiene by the ceramide desaturase FADS3, FASEB J. 34 (2020) 3318–3335. https://doi.org/10.1096/fj.201902645R.

[13] A. Ota, H. Morita, T. Naganuma, M. Miyamoto, K. Jojima, K. Nojiri, J. Matsuda, A. Kihara, Bifunctional DEGS2 has higher hydroxylase activity toward substrates with very-long-chain fatty acids in the production of phytosphingosine-ceramides, J. Biol. Chem. (2023) 104603. https://doi.org/10.1016/j.jbc.2023.104603.

[14] G. Karsai, M. Lone, Z. Kutalik, J.T. Brenna, H. Li, D. Pan, A. von Eckardstein, T. Hornemann, FADS3 is a Δ14Z sphingoid base desaturase that contributes to gender differences in the human plasma sphingolipidome, J. Biol. Chem. 295 (2020) 1889–1897. https://doi.org/10.1074/jbc.AC119.011883.

[15] P. Ternes, S. Franke, U. Zahringer, P. Sperling, E. Heinz, Identification and characterization of a sphingolipid Δ4-desaturase family, J. Biol. Chem. 277 (2002) 25512–25518. https://doi.org/10.1074/jbc.M202947200.

[16] L.F. Castro, D.R. Tocher, O. Monroig, Long-chain polyunsaturated fatty acid biosynthesis in chordates: Insights into the evolution of Fads and Elovl gene repertoire, Prog. Lipid Res. 62 (2016) 25–40. https://doi.org/10.1016/j.plipres.2016.01.001.

[17] H. Guillou, D. Zadravec, P.G. Martin, A. Jacobsson, The key roles of elongases and

desaturases in mammalian fatty acid metabolism: Insights from transgenic mice, Prog. Lipid Res. 49 (2010) 186–199. https://doi.org/10.1016/j.plipres.2009.12.002.

[18] R.A. Igal, D.I. Sinner, Stearoyl-CoA desaturase 5 (SCD5), a Δ-9 fatty acyl desaturase in search of a function, Biochim. Biophys. Acta Mol. Cell Biol. Lipids 1866 (2021) 158840. https://doi.org/10.1016/j.bbalip.2020.158840.

[19] F. Omae, M. Miyazaki, A. Enomoto, M. Suzuki, Y. Suzuki, A. Suzuki, DES2 protein is responsible for phytoceramide biosynthesis in the mouse small intestine, Biochem. J. 379 (2004) 687–695. https://doi.org/10.1042/BJ20031425.

[20] A. Marquardt, H. Stohr, K. White, B.H. Weber, cDNA cloning, genomic structure, and chromosomal localization of three members of the human fatty acid desaturase family, Genomics 66 (2000) 175–183. https://doi.org/10.1006/geno.2000.6196.

[21] Y. Michinaka, T. Aki, K. Inagaki, H. Higashimoto, Y. Shimada, T. Nakajima, T. Shimauchi, K. Ono, O. Suzuki, Production of polyunsaturated fatty acids by genetic engineering of yeast, J. Oleo Sci. 50 (2001) 359–365. https://doi.org/10.5650/jos.50.359.

[22] J. Duan, A.H. Merrill, Jr., 1-Deoxysphingolipids encountered exogenously and made *de novo*: Dangerous mysteries inside an enigma, J. Biol. Chem. 290 (2015) 15380–15389. https://doi.org/10.1074/jbc.R115.658823.

[23] G. Han, S.D. Gupta, K. Gable, S. Niranjanakumari, P. Moitra, F. Eichler, R.H. Brown, Jr., J.M. Harmon, T.M. Dunn, Identification of small subunits of mammalian serine palmitoyltransferase that confer distinct acyl-CoA substrate specificities, Proc. Natl. Acad. Sci. U. S. A. 106 (2009) 8186–8191. https://doi.org/10.1073/pnas.0811269106.

[24] J.M. Harmon, D. Bacikova, K. Gable, S.D. Gupta, G. Han, N. Sengupta, N. Somashekarappa, T.M. Dunn, Topological and functional characterization of the ssSPTs, small activating subunits of serine palmitoyltransferase, J. Biol. Chem. 288 (2013) 10144–10153. https://doi.org/10.1074/jbc.M113.451526.

[25] L. Zhao, S. Spassieva, K. Gable, S.D. Gupta, L.Y. Shi, J. Wang, J. Bielawski, W.L. Hicks,

M.P. Krebs, J. Naggert, Y.A. Hannun, T.M. Dunn, P.M. Nishina, Elevation of 20-carbon long chain bases due to a mutation in serine palmitoyltransferase small subunit b results in neurodegeneration, Proc. Natl. Acad. Sci. U. S. A. 112 (2015) 12962–12967. https://doi.org/10.1073/pnas.1516733112.

[26] M. Suzuki, Y. Ohno, A. Kihara, Whole picture of human stratum corneum ceramides, including the chain-length diversity of long-chain bases, J. Lipid Res. 63 (2022) 100235. https://doi.org/10.1016/j.jlr.2022.100235.

[27] F.S. Eichler, T. Hornemann, A. McCampbell, D. Kuljis, A. Penno, D. Vardeh, E. Tamrazian, K. Garofalo, H.J. Lee, L. Kini, M. Selig, M. Frosch, K. Gable, A. von Eckardstein, C.J. Woolf, G. Guan, J.M. Harmon, T.M. Dunn, R.H. Brown, Jr., Overexpression of the wild-type SPT1 subunit lowers desoxysphingolipid levels and rescues the phenotype of HSAN1, J. Neurosci. 29 (2009) 14646–14651. https://doi.org/10.1523/jneurosci.2536-09.2009.

[28] A. Penno, M.M. Reilly, H. Houlden, M. Laura, K. Rentsch, V. Niederkofler, E.T. Stoeckli, G. Nicholson, F. Eichler, R.H. Brown, Jr., A. von Eckardstein, T. Hornemann, Hereditary sensory neuropathy type 1 is caused by the accumulation of two neurotoxic sphingolipids, J. Biol. Chem. 285 (2010) 11178–11187. https://doi.org/10.1074/jbc.M109.092973.

[29] R. Steiner, E.M. Saied, A. Othman, C. Arenz, A.T. Maccarone, B.L. Poad, S.J. Blanksby, A. von Eckardstein, T. Hornemann, Elucidating the chemical structure of native 1-deoxysphingosine, J. Lipid Res. 57 (2016) 1194–1203. https://doi.org/10.1194/jlr.M067033.

[30] Y.A. Hannun, L.M. Obeid, Sphingolipids and their metabolism in physiology and disease, Nat. Rev. Mol. Cell Biol. 19 (2018) 175–191. https://doi.org/10.1038/nrm.2017.107.

[31] B.M. Quinville, N.M. Deschenes, A.E. Ryckman, J.S. Walia, A comprehensive review: sphingolipid metabolism and implications of disruption in sphingolipid homeostasis, Int. J. Mol. Sci. 22 (2021). https://doi.org/10.3390/ijms22115793.

[32] K. Nakahara, A. Ohkuni, T. Kitamura, K. Abe, T. Naganuma, Y. Ohno, R.A. Zoeller, A.

Kihara, The Sjögren-Larsson syndrome gene encodes a hexadecenal dehydrogenase of the sphingosine 1-phosphate degradation pathway, Mol. Cell 46 (2012) 461–471. https://doi.org/10.1016/j.molcel.2012.04.033.

[33] T. Naganuma, S. Takagi, T. Kanetake, T. Kitamura, S. Hattori, T. Miyakawa, T. Sassa, A. Kihara, Disruption of the Sjögren-Larsson syndrome gene *Aldh3a2* in mice increases keratinocyte growth and retards skin barrier recovery, J. Biol. Chem. 291 (2016) 11676–11688. https://doi.org/10.1074/jbc.M116.714030.

[34] N. Kondo, Y. Ohno, M. Yamagata, T. Obara, N. Seki, T. Kitamura, T. Naganuma, A. Kihara, Identification of the phytosphingosine metabolic pathway leading to odd-numbered fatty acids, Nat. Commun. 5 (2014) 5338. https://doi.org/10.1038/ncomms6338.

[35] T. Kitamura, N. Seki, A. Kihara, Phytosphingosine degradation pathway includes fatty acid α-oxidation reactions in the endoplasmic reticulum, Proc. Natl. Acad. Sci. U. S. A. 114 (2017) E2616–E2623. https://doi.org/10.1073/pnas.1700138114.

[36] M. Sawai, Y. Uchida, Y. Ohno, M. Miyamoto, C. Nishioka, S. Itohara, T. Sassa, A. Kihara, The 3-hydroxyacyl-CoA dehydratases HACD1 and HACD2 exhibit functional redundancy and are active in a wide range of fatty acid elongation pathways, J. Biol. Chem. 292 (2017) 15538–15551. https://doi.org/10.1074/jbc.M117.803171.

[37] A. Kihara, Y. Anada, Y. Igarashi, Mouse sphingosine kinase isoforms SPHK1a and SPHK1b differ in enzymatic traits including stability, localization, modification, and oligomerization, J. Biol. Chem. 281 (2006) 4532–4539. https://doi.org/10.1074/jbc.M510308200.

[38] M. Ikeda, Y. Kanao, M. Yamanaka, H. Sakuraba, Y. Mizutani, Y. Igarashi, A. Kihara, Characterization of four mammalian 3-hydroxyacyl-CoA dehydratases involved in very long-chain fatty acid synthesis, FEBS Lett. 582 (2008) 2435–2440. https://doi.org/10.1016/j.febslet.2008.06.007.

[39] Y. Ohno, S. Suto, M. Yamanaka, Y. Mizutani, S. Mitsutake, Y. Igarashi, T. Sassa, A. Kihara,

ELOVL1 production of C24 acyl-CoAs is linked to C24 sphingolipid synthesis, Proc. Natl. Acad. Sci. U. S. A. 107 (2010) 18439–18444. https://doi.org/10.1073/pnas.1005572107.

[40] Y. Mizutani, A. Kihara, Y. Igarashi, Mammalian Lass6 and its related family members regulate synthesis of specific ceramides, Biochem. J. 390 (2005) 263–271. https://doi.org/10.1042/BJ20050291.

[41] Y. Mizutani, A. Kihara, Y. Igarashi, LASS3 (longevity assurance homologue 3) is a mainly testis-specific (dihydro)ceramide synthase with relatively broad substrate specificity, Biochem. J. 398 (2006) 531–538. https://doi.org/10.1042/BJ20060379.

[42] R. Tidhar, A.H. Futerman, The complexity of sphingolipid biosynthesis in the endoplasmic reticulum, Biochim. Biophys. Acta 1833 (2013) 2511–2518. https://doi.org/10.1016/j.bbamcr.2013.04.010.

[43] T. Sassa, T. Hirayama, A. Kihara, Enzyme activities of the ceramide synthases CERS2–6 are regulated by phosphorylation in the C-terminal region, J. Biol. Chem. 291 (2016) 7477–7487. https://doi.org/10.1074/jbc.M115.695858.

[44] T. Sassa, Y. Ohno, S. Suzuki, T. Nomura, C. Nishioka, T. Kashiwagi, T. Hirayama, M. Akiyama, R. Taguchi, H. Shimizu, S. Itohara, A. Kihara, Impaired epidermal permeability barrier in mice lacking *Elovl1*, the gene responsible for very-long-chain fatty acid production, Mol. Cell. Biol. 33 (2013) 2787–2796. https://doi.org/10.1128/MCB.00192-13.

[45] M. Yamamoto, T. Sassa, Y. Kyono, H. Uemura, M. Kugo, H. Hayashi, Y. Imai, K. Yamanishi, A. Kihara, Comprehensive stratum corneum ceramide profiling reveals reduced acylceramides in ichthyosis patient with *CERS3* mutations, J. Dermatol. 48 (2021) 447–456. https://doi.org/10.1111/1346-8138.15725.

[46] A. Rosenberg, N. Stern, Changes in sphingosine and fatty acid components of the gangliosides in developing rat and human brain, J. Lipid Res. 7 (1966) 122–131.

[47] M.A. Lone, A.J. Hulsmeier, E.M. Saied, G. Karsai, C. Arenz, A. von Eckardstein, T.

Hornemann, Subunit composition of the mammalian serine-palmitoyltransferase defines the spectrum of straight and methyl-branched long-chain bases, Proc. Natl. Acad. Sci. U. S. A. 117 (2020) 15591–15598. https://doi.org/10.1073/pnas.2002391117.

[48] H. Tanno, T. Sassa, M. Sawai, A. Kihara, Production of branched-chain very-long-chain fatty acids by fatty acid elongases and their tissue distribution in mammals, Biochim. Biophys. Acta Mol. Cell Biol. Lipids 1866 (2021) 158842. https://doi.org/10.1016/j.bbalip.2020.158842.

[49] G. Karsai, F. Kraft, N. Haag, G.C. Korenke, B. Hanisch, A. Othman, S. Suriyanarayanan, R. Steiner, C. Knopp, M. Mull, M. Bergmann, J.M. Schroder, J. Weis, M. Elbracht, M. Begemann, T. Hornemann, I. Kurth, DEGS1-associated aberrant sphingolipid metabolism impairs nervous system function in humans, J. Clin. Invest. 129 (2019) 1229–1239. https://doi.org/10.1172/JCI124159.

[50] F. Lederer, R. Ghrir, B. Guiard, S. Cortial, A. Ito, Two homologous cytochromes b_5 in a single cell, Eur. J. Biochem. 132 (1983) 95–102. https://doi.org/10.1111/j.1432-1033.1983.tb07330.x.

[51] T. Wakashima, K. Abe, A. Kihara, Dual functions of the *trans*-2-enoyl-CoA reductase TER in the sphingosine 1-phosphate metabolic pathway and in fatty acid elongation, J. Biol. Chem. 289 (2014) 24736–24748. https://doi.org/10.1074/jbc.M114.571869.

[52] H. Wang, M.G. Klein, H. Zou, W. Lane, G. Snell, I. Levin, K. Li, B.C. Sang, Crystal structure of human stearoyl-coenzyme A desaturase in complex with substrate, Nat. Struct. Mol. Biol. 22 (2015) 581–585. https://doi.org/10.1038/nsmb.3049.

[53] H.G. Enoch, A. Catala, P. Strittmatter, Mechanism of rat liver microsomal stearyl-CoA desaturase. Studies of the substrate specificity, enzyme-substrate interactions, and the function of lipid, J. Biol. Chem. 251 (1976) 5095–5103.

[54] Y. Bai, J.G. McCoy, E.J. Levin, P. Sobrado, K.R. Rajashankar, B.G. Fox, M. Zhou, X-ray structure of a mammalian stearoyl-CoA desaturase, Nature 524 (2015) 252–256.

https://doi.org/10.1038/nature14549.

[55] T. Okayasu, M. Nagao, T. Ishibashi, Y. Imai, Purification and partial characterization of linoleoyl-CoA desaturase from rat liver microsomes, Arch. Biochem. Biophys. 206 (1981) 21–28. https://doi.org/10.1016/0003-9861(81)90061-8.

[56] C.M. Paton, J.M. Ntambi, Biochemical and physiological function of stearoyl-CoA desaturase, Am. J. Physiol. Endocrinol. Metab. 297 (2009) E28–37. https://doi.org/10.1152/ajpendo.90897.2008.

[57] N. Oshino, Y. Imai, R. Sato, A function of cytochrome b_5 in fatty acid desaturation by rat liver microsomes, J. Biochem. 69 (1971) 155–167. https://doi.org/10.1093/oxfordjournals.jbchem.a129444.

[58] T.D. Porter, The roles of cytochrome b_5 in cytochrome P450 reactions, J. Biochem. Mol. Toxicol. 16 (2002) 311–316. https://doi.org/10.1002/jbt.10052.

Figure captions

Fig. 1. The substrates of FADS3 are SPH-CERs only, not SPH. (A, B) HEK 293T cells were transfected with empty vector (pCE-puro 3×FLAG-1) or the plasmid expressing 3×FLAG-FADS3 (pCE-puro 3×FLAG-FADS3). (A) Twenty-four hours after transfection, cells were treated with 20 μM FB_1 for 6 h and then labeled with 1 μM d_7-SPH for 4 h. Lipids were extracted from the cells, and d_7-SPH-CERs, d_7-SPD-CERs, d_7-SPH, and d_7-SPD were quantified via LC-MS/MS. The values presented for d_7-SPH-CERs and d_7-SPD-CERs are the sums of the quantities of species with C16:0, C18:0, C20:0, C22:0, C24:1, and C24:0 in the FA moiety. Bars indicate means + SD (n = 3) with white circles representing each individual value. Statistical significance (Tukey's test) is indicated only for the differences between the vector and *FADS3* (## $p < 0.01$) and between those with and without FB_1 (** $p < 0.01$). ND, not detected. (B) Twenty-four hours after transfection, total cell lysates were prepared and incubated with 10 μM d_7-SPH or C6-SPH-CER in the presence of 1 mM NADH at 37 °C for 10 min. Lipids were extracted, and d_7-SPD and C6-SPD-CER were quantified via LC-MS/MS. Values presented are means + SD (n = 3; ** $p < 0.01$; Student's *t*-test).

Fig. 2. FADS3 shows no specificity with respect to the FA chain length of SPH-CERs. (A–D) HEK 293T cells were transfected with empty vector (pCE-puro 3×FLAG-1; A–D) and the plasmids expressing 3×FLAG-CERS isozymes (A and B, CERS1–6; C and D, CERS3), 3×FLAG-ELOVL1 (C and D), and 3×FLAG-FADS3 (A–D) in the combination shown in the figure. (A, C) Twenty-four hours after transfection, total cell lysates were prepared and subjected to immunoblotting using anti-FLAG and anti-GAPDH (loading control) antibodies. IB, immunoblotting. (B, D) Twenty-four hours after transfection, cells were labeled with 1 μM d_7-SPH for 4 h. Lipids were extracted from the cells, and d_7-SPH-CERs and d_7-SPD-CERs were quantified via LC-MS/MS. Values presented are means + SD of the total quantities of d_7-SPH-CERs or d_7-SPD-CERs, with FA species color coded (n = 3; * $p < 0.05$; ** $p < 0.01$;

Student's *t*-test; vector vs *FADS3*).

Fig. 3. FADS3 shows specificity with respect to chain length and chain branching in the LCB moiety of SPH-CERs. (A–D) HEK 293T cells were transfected with empty vector (pCE-puro 3×FLAG-1) and the plasmids expressing 3×FLAG-SPTLC1, 3×FLAG-SPTSSB, HA-SPTLC3, and 3×FLAG-FADS3 in the combination shown in the figure. Cells were then cultured for 24 h. (A) Total cell lysates were prepared and subjected to immunoblotting using anti-FLAG, anti-HA, and anti-GAPDH (loading control) antibodies. IB, immunoblotting. (B, C) Lipids were extracted, and SPH-CERs and SPD-CERs with chain lengths of d16–d24 were quantified via LC-MS/MS. (B) The values presented for SPH-CERs and SPD-CERs are the sums of the quantities of species with C16:0, C18:0, C20:0, C22:0, C24:1, and C24:0 in the FA moiety. Values presented are means + SD (n = 3; * $p < 0.05$; ** $p < 0.01$; Student's *t*-test). (C) Ion chromatograms of SPH-CER (d19:1/C24:0) and SPD-CER (d19:2/C24:0) are shown. Asterisks represent nonspecific backgrounds. (D) Cells were treated with 25 μM straight-chain, *iso*-branched-chain, or *anteiso*-branched-chain FAs (all C17:0) for 8 h. Lipids were extracted and d19:1 SPH-CERs and d19:2 SPD-CERs with straight-chain, *iso*-branched-chain, or *anteiso*-branched-chain LCB were quantified via LC-MS/MS. The values presented for d19:1 SPH-CERs and d19:2 SPD-CERs are the sums of the quantities of species with C16:0, C18:0, C20:0, C22:0, C24:1, and C24:0 in the FA moiety. Values presented are means + SD (n = 3; ** $p < 0.01$; Dunnet's test; vs ethanol).

Fig. 4. FADS3 shows activity toward DHS-CERs. (A, B) *DEGS1* KO HAP1 cells were transfected with empty vector (pCE-puro 3×FLAG-1) or the plasmid expressing 3×FLAG-FADS3 (pCE-puro 3×FLAG-FADS3). Cells were then cultured for 24 h. (A) Cells were labeled with 2 μM d_7-DHS for 4 h. Lipids were extracted from the cells, and d_7-14*Z*-SPH-CERs were quantified via LC-MS/MS. The values presented are the sums of the quantities of d_7-14*Z*-SPH-

CER species with C16:0, C18:0, C20:0, C22:0, C24:1, and C24:0 in the FA moiety. Values presented are means + SD (n = 3; ** $p < 0.01$; Student's *t*-test). (B) Total cell lysates were prepared and incubated with 10 μM C6-SPH-CER or C6-DHS-CER in the presence of 1 mM NADH at 37 °C for 10 min. Lipids were extracted, and C6-SPD-CER and C6-14*Z*-SPH-CER were quantified via LC-MS/MS. Values presented are means + SD (n = 3; ** $p < 0.01$; Tukey's test). (C) Two possible DHS-CER-to-SPD-CER synthesis pathways are shown: one via SPH-CER and the other via 14*Z*-SPH-CER. *D*, *DEGS1* KO HAP1 cells were cultured in serum- and antibiotic-free medium for 24 h. The medium was then replaced with one containing 10 mg/mL FA-free BSA and 1 μM 14*Z*-SPH. After four hours of incubation, the lipids were extracted from the cells and SPD-CERs and 14*Z*-SPH-CERs were quantified via LC-MS/MS. The values presented are the sums of the quantities of SPD-CER or 14*Z*-SPH-CER species with C16:0, C18:0, C20:0, C22:0, C24:1, and C24:0 in the FA moiety. Values represent means + SD (n = 3; ** $p < 0.01$; Tukey's test).

Fig. 5. Cytochrome b_5 promotes the reaction catalyzed by FADS3. (A) HEK 293T cells were transfected with the plasmid expressing 3×FLAG-FADS3 (pCE-puro 3×FLAG-FADS3). Twenty-four hours after transfection, total cell lysates were prepared and incubated with C6-SPH-CER in the presence or absence of 1 mM NADH or NADPH. Lipids were extracted, and C6-SPD-CER was quantified via LC-MS/MS. Values presented are means + SD (n = 3; ** $p < 0.01$; Tukey's test). (B, C) HEK 293T cells were transfected with empty vector (pCE-puro 3×FLAG-1) or the plasmid expressing 3×FLAG-CYB5A together with the plasmid expressing 3×FLAG-FADS3 and cultured for 24 h. (B) Total cell lysates were prepared and subjected to immunoblotting using anti-FLAG and anti-GAPDH (loading control) antibodies. IB, immunoblotting. (C) Cells were labeled with 1 μM d_7-SPH for 4 h. Lipids were extracted, and d_7-SPD-CERs were quantified via LC-MS/MS. The values presented are the sums of the quantities of d_7-SPD-CER species with C16:0, C18:0, C20:0, C22:0, C24:1, and C24:0 in the

FA moiety. Values presented are means + SD (n = 3; ** $p < 0.01$; Student's *t*-test).

Fig. 6. SPD is predominantly metabolized to SMs rather than HexCERs. (A) *FADS3* KO HAP1 cells were labeled with 5 μM d_7-SPH or d_7-SPD for 0, 1, 5, 10, or 24 h. Lipids were extracted from the cells, and d_7-labeled CERs, HexCERs, and SMs were quantified via LC-MS/MS. The values presented are the sums of the quantities of individual species with C16:0, C18:0, C20:0, C22:0, C24:1, and C24:0 in the FA moiety. Values presented are means ± SD (n = 3; * $p < 0.05$; ** $p < 0.01$; Student's *t*-test). (B) Lipids were extracted from brain and kidney of three-month-old male mice (n = 3) and the quantities of CERs, SMs, and HexCERs containing d18:1 SPH or d18:2 SPD were quantified via LC-MS/MS. The values presented are the means + SD of the sums of the quantities of individual species with C16:0, C18:0, C20:0, C22:0, C24:1, and C24:0 in the FA moiety.

Fig. 7. SPD is metabolized to mono-unsaturated acyl-CoAs/FAs. (A) The metabolism pathways of DHS, SPH, and PHS are illustrated. LCBs are metabolized to acyl-CoAs via four common steps: C1 phosphorylation, C2–C3 cleavage, oxidation, and CoA addition. In addition, SPH and PHS undergo reduction (saturation) and α-oxidation (cleavage, oxidation, and CoA addition), respectively. Through these reactions, DHS (d[*x*]:0), SPH (d[*x*]:1), and PHS (t[*x*]:0) are metabolized to acyl-CoAs with C[$x - 2$]:0, C[$x - 2$]:0, and C[$x - 3$]:0, respectively. These acyl-CoAs are then mainly used for glycerophospholipid synthesis, either directly or after elongation and/or desaturation. (B) *FADS3* KO HAP1 cells were labeled with 5 μM d_7-SPH or d_7-SPD for 0, 1, 5, 10, or 24 h. Lipids were extracted from cells and subjected to alkali treatment to release the FAs from the glycerolipids. The FAs were then derivatized with *N*-(4-aminomethylphenyl) pyridinium, and d_7-FAs (C16:2, C18:2, C20:2, C16:1, C18:1, C20:1, C16:0, C18:0, and C20:0) were quantified via LC-MS/MS. Values presented are means + SD of the total quantities of d_7-FAs, with the FA species color coded (n = 3; * $p < 0.05$; Student's

t-test). (C) d_7-C16:1 FA generated in *FADS3* KO HAP1 cells treated with d_7-SPD for 10 h and commercially available *cis*-9- and *trans*-2-C16:1 FAs were derivatized with *N*-(4-aminomethylphenyl) pyridinium and subjected to LC-MS/MS. Their ion chromatograms are shown. (D) The proposed metabolic pathway of SPD (d[*x*]:2) to acyl-CoA (C[$x - 2$]:1) is illustrated. SPD undergoes the four reactions common to LCBs, and the resulting di-unsaturated acyl-CoA is converted to mono-unsaturated acyl-CoA via saturation of the *trans*-double bond at C2 (corresponding to C4 in SPD).

Figure 1

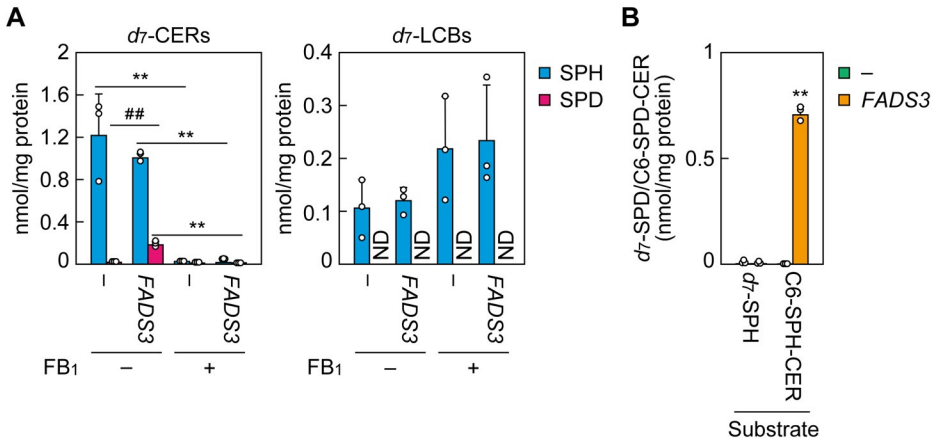
A
d7-CERs
d7-LCBs
nmol/mg protein
SPH
SPD
ND
FADS3
FB1
B
d7-SPD/C6-SPD-CER (nmol/mg protein)
d7-SPH
C6-SPH-CER
Substrate

Figure 2

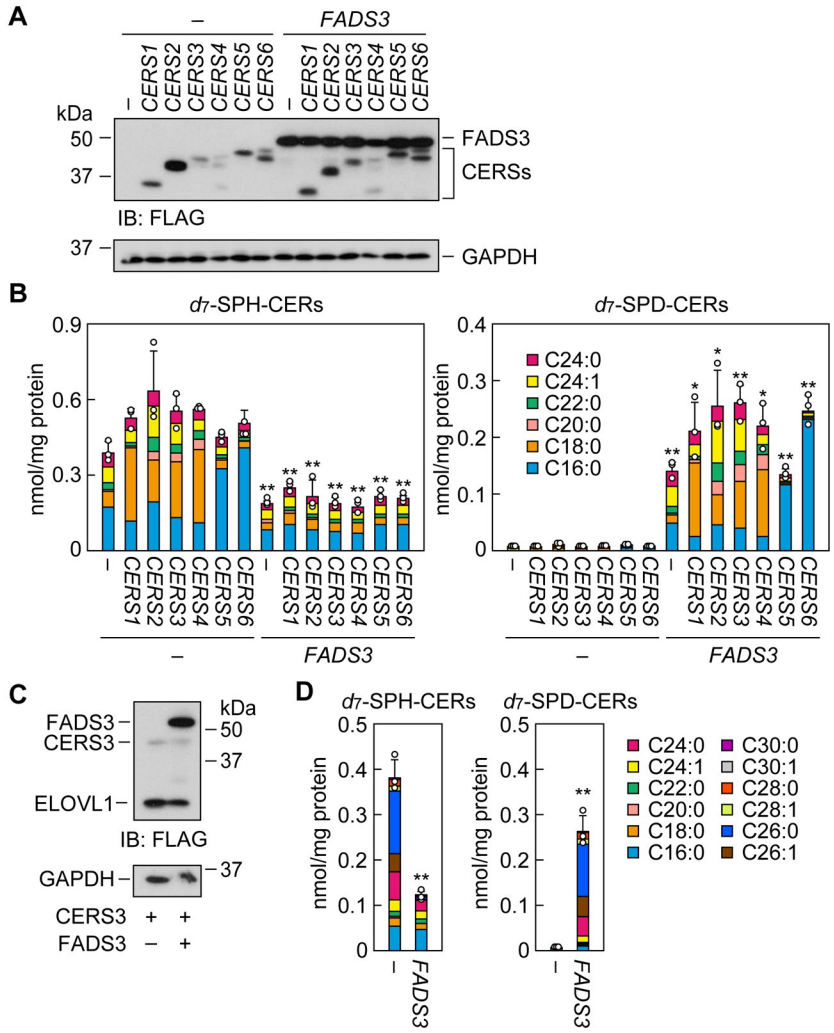
A
–
FADS3
– CERS1 CERS2 CERS3 CERS4 CERS5 CERS6 – CERS1 CERS2 CERS3 CERS4 CERS5 CERS6
kDa
50
37
FADS3
CERSs
IB: FLAG
37
GAPDH
B
d7-SPH-CERs
d7-SPD-CERs
nmol/mg protein
C24:0
C24:1
C22:0
C20:0
C18:0
C16:0
– CERS1 CERS2 CERS3 CERS4 CERS5 CERS6 – CERS1 CERS2 CERS3 CERS4 CERS5 CERS6
–
FADS3
C
FADS3
CERS3
ELOVL1
kDa
50
37
IB: FLAG
GAPDH
37
CERS3 + +
FADS3 – +
D
d7-SPH-CERs
d7-SPD-CERs
nmol/mg protein
C24:0
C24:1
C22:0
C20:0
C18:0
C16:0
C30:0
C30:1
C28:0
C28:1
C26:0
C26:1
– FADS3

Figure 3

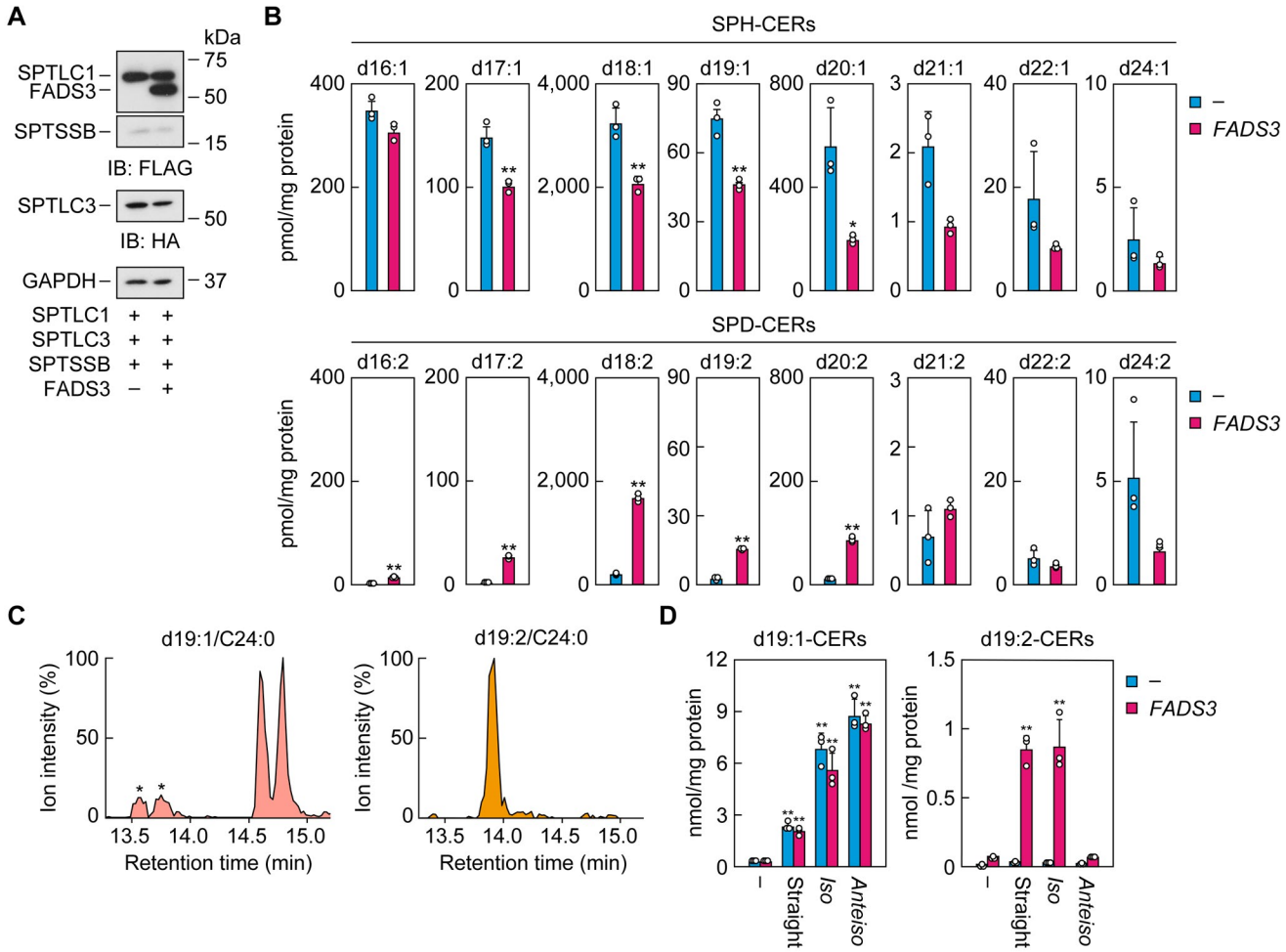
A
kDa
SPTLC1
FADS3
75
50
SPTSSB
15
IB: FLAG
SPTLC3
50
IB: HA
GAPDH
37
SPTLC1 + +
SPTLC3 + +
SPTSSB + +
FADS3 – +
B
SPH-CERs
d16:1
d17:1
d18:1
d19:1
d20:1
d21:1
d22:1
d24:1
pmol/mg protein
SPD-CERs
d16:2
d17:2
d18:2
d19:2
d20:2
d21:2
d22:2
d24:2
–
FADS3
C
d19:1/C24:0
d19:2/C24:0
Ion intensity (%)
Retention time (min)
D
d19:1-CERs
d19:2-CERs
nmol/mg protein
Straight
Iso
Anteiso

Figure 4

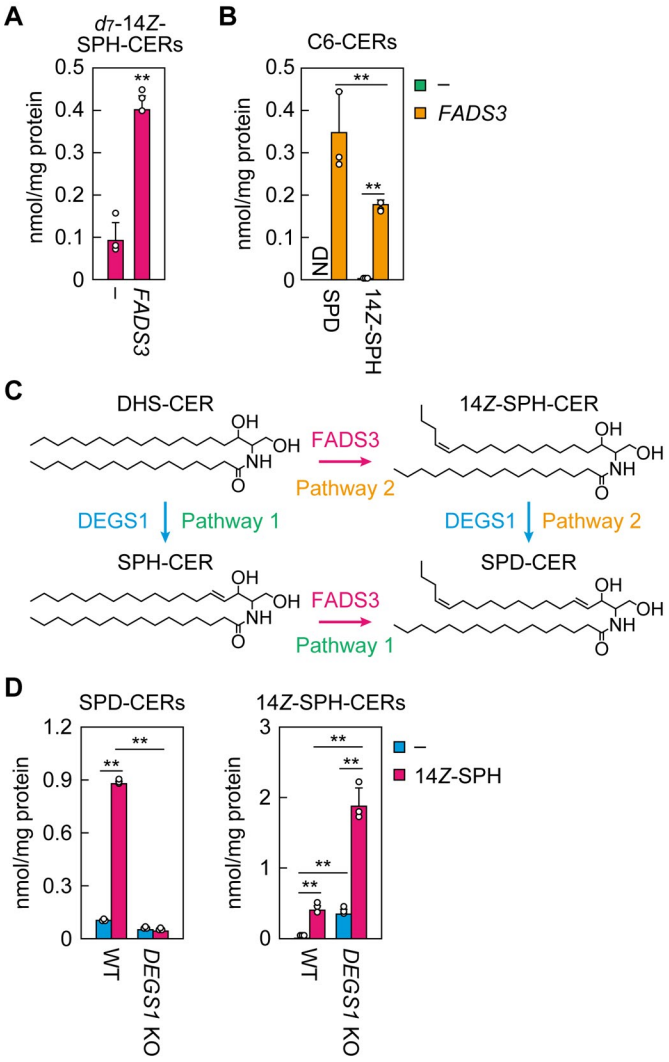
A
d7-14Z-SPH-CERs
nmol/mg protein
0.5
0.4
0.3
0.2
0.1
0
**
–
FADS3
B
C6-CERs
nmol/mg protein
0.5
0.4
0.3
0.2
0.1
0
**
**
ND
SPD
14Z-SPH
–
FADS3
C
DHS-CER
OH
OH
NH
O
FADS3
Pathway 2
14Z-SPH-CER
DEGS1
Pathway 1
DEGS1
Pathway 2
SPH-CER
FADS3
Pathway 1
SPD-CER
D
SPD-CERs
nmol/mg protein
1.2
0.9
0.6
0.3
0
**
**
WT
DEGS1 KO
14Z-SPH-CERs
nmol/mg protein
3
2
1
0
**
**
**
**
WT
DEGS1 KO
–
14Z-SPH

Figure 5

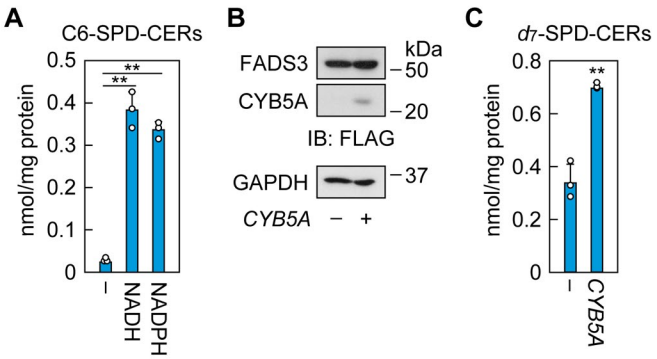
A
C6-SPD-CERs
nmol/mg protein
0.5
0.4
0.3
0.2
0.1
0
**
**
–
NADH
NADPH
B
kDa
FADS3
50
CYB5A
20
IB: FLAG
GAPDH
37
CYB5A – +
C
d7-SPD-CERs
nmol/mg protein
0.8
0.6
0.4
0.2
0
**
–
CYB5A

Figure 6

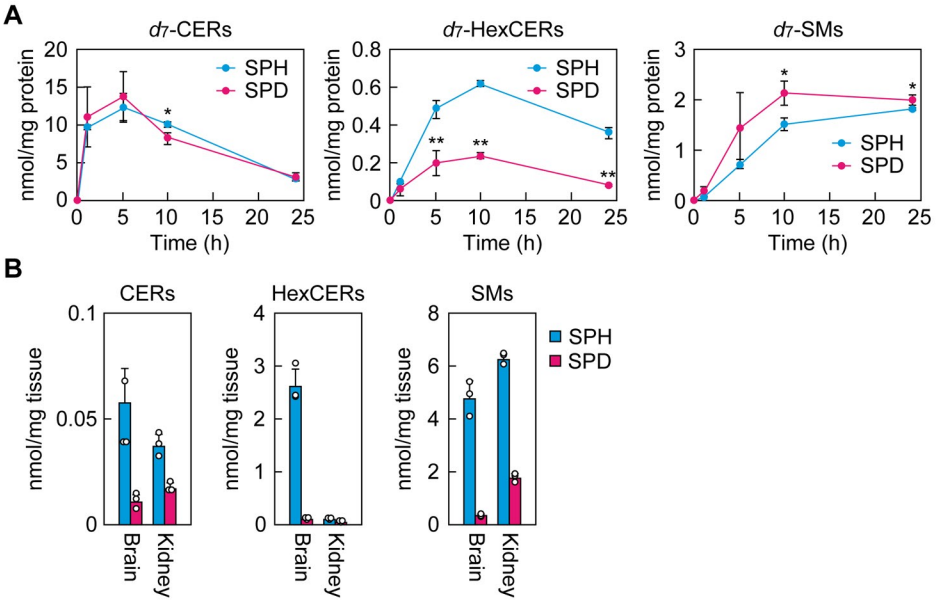
A
d7-CERs
d7-HexCERs
d7-SMs
nmol/mg protein
Time (h)
SPH
SPD
B
CERs
HexCERs
SMs
nmol/mg tissue
Brain
Kidney

Figure 7

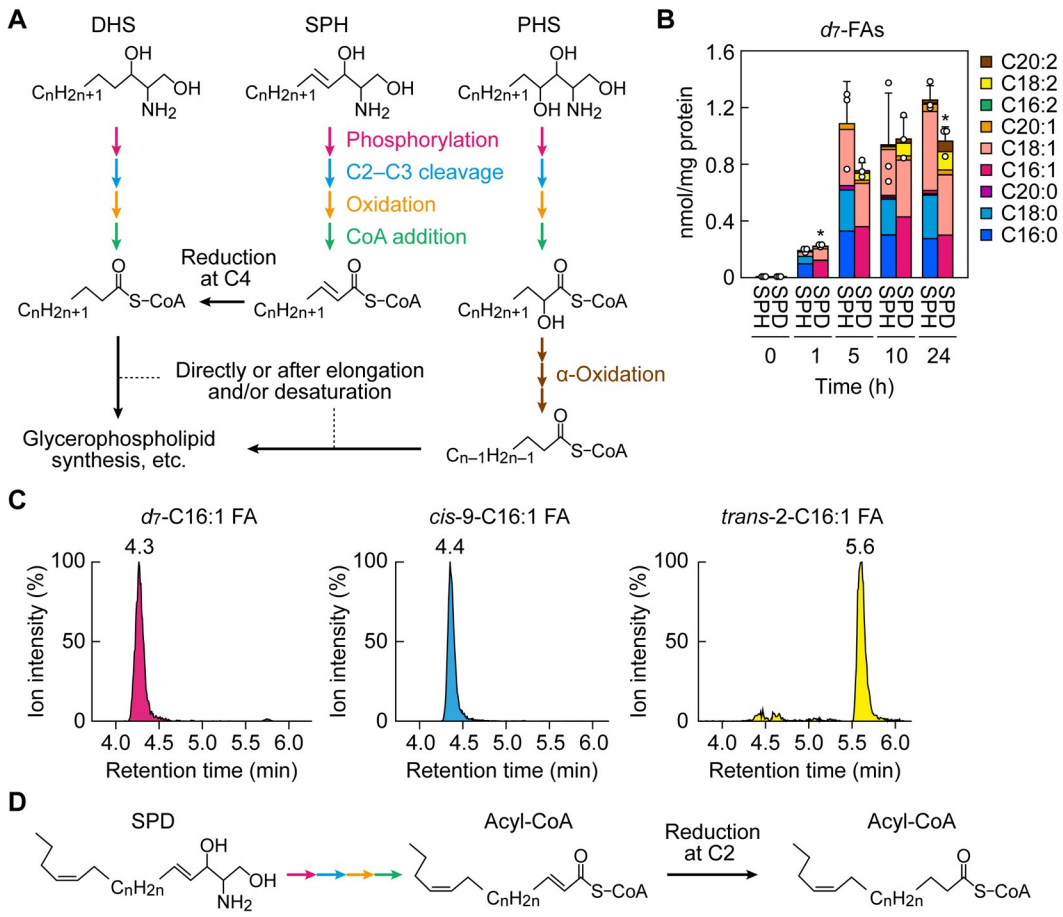
A
DHS
SPH
PHS
Phosphorylation
C2–C3 cleavage
Oxidation
CoA addition
Reduction at C4
Directly or after elongation and/or desaturation
α-Oxidation
Glycerophospholipid synthesis, etc.
B
d7-FAs
nmol/mg protein
Time (h)
C20:2
C18:2
C16:2
C20:1
C18:1
C16:1
C20:0
C18:0
C16:0
C
d7-C16:1 FA
cis-9-C16:1 FA
trans-2-C16:1 FA
Ion intensity (%)
Retention time (min)
4.3
4.4
5.6
D
SPD
Acyl-CoA
Reduction at C2

Table S1. MRM settings used in LC-MS/MS analyses

Lipid class	Species	Precursor ion	Q1 value	Q3 value	Collision energy (eV)
CER	d_7-d18:1/C16:0	$[M–H_2O + H]^+$	527.5	271.3	20
CER	d_7-d18:1/C18:0	$[M–H_2O + H]^+$	555.6	271.3	20
CER	d_7-d18:1/C20:0	$[M–H_2O + H]^+$	583.6	271.3	20
CER	d_7-d18:1/C22:0	$[M–H_2O + H]^+$	611.6	271.3	25
CER	d_7-d18:1/C24:1	$[M–H_2O + H]^+$	637.6	271.3	30
CER	d_7-d18:1/C24:0	$[M–H_2O + H]^+$	639.6	271.3	30
CER	d_7-d18:1/C26:1	$[M–H_2O + H]^+$	665.6	271.3	30
CER	d_7-d18:1/C26:0	$[M–H_2O + H]^+$	667.6	271.3	30
CER	d_7-d18:1/C28:1	$[M–H_2O + H]^+$	693.6	271.3	30
CER	d_7-d18:1/C28:0	$[M–H_2O + H]^+$	695.6	271.3	30
CER	d_7-d18:1/C30:1	$[M–H_2O + H]^+$	721.6	271.3	35
CER	d_7-d18:1/C30:0	$[M–H_2O + H]^+$	723.6	271.3	35
CER	d_7-d18:2/C16:0	$[M–H_2O + H]^+$	525.5	269.3	20
CER	d_7-d18:2/C18:0	$[M–H_2O + H]^+$	553.6	269.3	20
CER	d_7-d18:2/C20:0	$[M–H_2O + H]^+$	581.6	269.3	20
CER	d_7-d18:2/C22:0	$[M–H_2O + H]^+$	609.6	269.3	25
CER	d_7-d18:2/C24:1	$[M–H_2O + H]^+$	635.6	269.3	30
CER	d_7-d18:2/C24:0	$[M–H_2O + H]^+$	637.6	269.3	30
CER	d_7-d18:2/C26:1	$[M–H_2O + H]^+$	663.6	269.3	30
CER	d_7-d18:2/C26:0	$[M–H_2O + H]^+$	665.6	269.3	30
CER	d_7-d18:2/C28:1	$[M–H_2O + H]^+$	691.6	269.3	30
CER	d_7-d18:2/C28:0	$[M–H_2O + H]^+$	693.6	269.3	30
CER	d_7-d18:2/C30:1	$[M–H_2O + H]^+$	719.6	269.3	35
CER	d_7-d18:2/C30:0	$[M–H_2O + H]^+$	721.6	269.3	35
CER	d18:1(14Z)/C16:0	$[M + H]^+$	538.5	282.3	20
CER	d18:1(14Z)/C18:0	$[M + H]^+$	566.6	282.3	20
CER	d18:1(14Z)/C20:0	$[M + H]^+$	594.6	282.3	20
CER	d18:1(14Z)/C22:0	$[M + H]^+$	622.6	282.3	25
CER	d18:1(14Z)/C24:1	$[M + H]^+$	648.6	282.3	30
CER	d18:1(14Z)/C24:0	$[M + H]^+$	650.6	282.3	30
CER	d_7-d18:1(14*Z*)/C16:0	$[M + H]^+$	803.6	269.3	20

CER	d_7-d18:1(14*Z*)/C18:0	$[M + H]^+$	545.5	289.3	20
CER	d_7-d18:1(14*Z*)/C20:0	$[M + H]^+$	573.6	289.3	20
CER	d_7-d18:1(14*Z*)/C22:0	$[M + H]^+$	601.6	289.3	25
CER	d_7-d18:1(14*Z*)/C24:1	$[M + H]^+$	627.6	289.3	30
CER	d_7-d18:1(14*Z*)/C24:0	$[M + H]^+$	629.6	289.3	30
HexCer	d18:1/C16:0	$[M–H_2O + H]^+$	682.6	264.3	40
HexCer	d18:1/C18:0	$[M–H_2O + H]^+$	710.6	264.3	40
HexCer	d18:1/C20:0	$[M–H_2O + H]^+$	738.6	264.3	40
HexCer	d18:1/C22:0	$[M–H_2O + H]^+$	766.6	264.3	40
HexCer	d18:1/C24:0	$[M–H_2O + H]^+$	794.7	264.3	40
HexCer	d18:2/C16:0	$[M–H_2O + H]^+$	680.6	262.3	40
HexCer	d18:2/C18:0	$[M–H_2O + H]^+$	708.6	262.3	40
HexCer	d18:2/C20:0	$[M–H_2O + H]^+$	736.6	262.3	40
HexCer	d18:2/C22:0	$[M–H_2O + H]^+$	764.6	262.3	40
HexCer	d18:2/C24:0	$[M–H_2O + H]^+$	792.7	262.3	40
HexCer	d_7-d18:1/C16:0	$[M–H_2O + H]^+$	689.6	271.3	40
HexCer	d_7-d18:1/C18:0	$[M–H_2O + H]^+$	717.6	271.3	40
HexCer	d_7-d18:1/C20:0	$[M–H_2O + H]^+$	745.6	271.3	40
HexCer	d_7-d18:1/C22:0	$[M–H_2O + H]^+$	773.6	271.3	40
HexCer	d_7-d18:1/C24:1	$[M–H_2O + H]^+$	799.7	271.3	40
HexCer	d_7-d18:1/C24:0	$[M–H_2O + H]^+$	801.7	271.3	40
HexCer	d_7-d18:2/C16:0	$[M–H_2O + H]^+$	687.6	269.3	40
HexCer	d_7-d18:2/C18:0	$[M–H_2O + H]^+$	715.6	269.3	40
HexCer	d_7-d18:2/C20:0	$[M–H_2O + H]^+$	743.6	269.3	40
HexCer	d_7-d18:2/C22:0	$[M–H_2O + H]^+$	771.6	269.3	40
HexCer	d_7-d18:2/C24:1	$[M–H_2O + H]^+$	797.7	269.3	40
HexCer	d_7-d18:2/C24:0	$[M–H_2O + H]^+$	799.7	269.3	40
SM	d18:1/C16:0	$[M + H]^+$	703.7	184.2	60
SM	d18:1/C18:0	$[M + H]^+$	731.7	184.2	60
SM	d18:1/C20:0	$[M + H]^+$	759.8	184.2	60
SM	d18:1/C22:0	$[M + H]^+$	787.8	184.2	60
SM	d18:1/C24:0	$[M + H]^+$	815.8	184.2	60
SM	d18:2/C16:0	$[M + H]^+$	701.7	184.2	60
SM	d18:2/C18:0	$[M + H]^+$	729.7	184.2	60

SM	d18:2/C20:0	$[M + H]^+$	757.8	184.2	60
SM	d18:2/C22:0	$[M + H]^+$	785.8	184.2	60
SM	d18:2/C24:0	$[M + H]^+$	813.8	184.2	60
SM	d_7-d18:1/C16:0	$[M + H]^+$	710.7	184.2	60
SM	d_7-d18:1/C18:0	$[M + H]^+$	738.7	184.2	60
SM	d_7-d18:1/C20:0	$[M + H]^+$	766.8	184.2	60
SM	d_7-d18:1/C22:0	$[M + H]^+$	794.8	184.2	60
SM	d_7-d18:1/C24:1	$[M + H]^+$	820.8	184.2	60
SM	d_7-d18:1/C24:0	$[M + H]^+$	822.8	184.2	60
SM	d_7-d18:2/C16:0	$[M + H]^+$	708.7	184.2	60
SM	d_7-d18:2/C18:0	$[M + H]^+$	736.7	184.2	60
SM	d_7-d18:2/C20:0	$[M + H]^+$	764.8	184.2	60
SM	d_7-d18:2/C22:0	$[M + H]^+$	792.8	184.2	60
SM	d_7-d18:2/C24:1	$[M + H]^+$	818.8	184.2	60
SM	d_7-d18:2/C24:0	$[M + H]^+$	820.8	184.2	60
SPH	d_7-d18:1	$[M–H_2O + H]^+$	289.3	271.3	15
SPD	d_7-d18:2	$[M–H_2O + H]^+$	287.2	269.2	15
FA	C16:1	$[M +AMPP]^+$	421.4	239.0	48
FA	d_7-C16:3	$[M +AMPP]^+$	424.4	239.0	48
FA	d_7-C16:2	$[M +AMPP]^+$	426.4	239.0	48
FA	d_7-C16:1	$[M +AMPP]^+$	428.4	239.0	48
FA	d_7-C16:0	$[M +AMPP]^+$	430.4	239.0	50
FA	d_7-C18:3	$[M +AMPP]^+$	452.4	239.0	44
FA	d_7-C18:2	$[M +AMPP]^+$	454.4	239.0	44
FA	d_7-C18:1	$[M +AMPP]^+$	456.4	239.0	48
FA	d_7-C18:0	$[M +AMPP]^+$	458.4	239.0	50
FA	d_7-C20:3	$[M +AMPP]^+$	480.4	239.0	48
FA	d_7-C20:2	$[M +AMPP]^+$	482.4	239.0	48
FA	d_7-C20:1	$[M +AMPP]^+$	484.4	239.0	48
FA	d_7-C20:0	$[M +AMPP]^+$	486.4	239.0	50

AMPP: *N*-(4-aminomethylphenyl) pyridinium.